Microscopic derivation of multichannel Hubbard models for ultracold nonreactive molecules in an optical lattice

Michael L. Wall,[1,*] Nirav P. Mehta,[2] Rick Mukherjee,[3,4] Shah Saad Alam,[3,4] and Kaden R. A. Hazzard[3,4,†]

[1]*JILA, NIST and University of Colorado, Boulder, Colorado 80309, USA*

[2]*Department of Physics and Astronomy, Trinity University, San Antonio, Texas 78212, USA*

[3]*Department of Physics and Astronomy, Rice University, Houston, Texas 77005, USA*

[4]*Rice Center for Quantum Materials, Rice University, Houston, Texas 77005, USA*

(Received 21 December 2016; published 25 April 2017)

Recent experimental advances in the cooling and manipulation of bialkali-metal dimer molecules have enabled the production of gases of ultracold molecules that are not chemically reactive. It has been presumed in the literature that in the absence of an electric field the low-energy scattering of such nonreactive molecules (NRMs) will be similar to atoms, in which a single s-wave scattering length governs the collisional physics. However, Doçaj *et al.* [Phys. Rev. Lett. **116**, 135301 (2016)] argued that the short-range collisional physics of NRMs is much more complex than for atoms and that this leads to a many-body description in terms of a multichannel Hubbard model. In this work we show that this multichannel Hubbard model description of NRMs in an optical lattice is robust against the approximations employed by Doçaj *et al.* to estimate its parameters. We do so via an exact, albeit formal, derivation of a multichannel resonance model for two NRMs from an *ab initio* description of the molecules in terms of their constituent atoms. We discuss the regularization of this two-body multichannel resonance model in the presence of a harmonic trap and how its solutions form the basis for the many-body model of Doçaj *et al.*. We also generalize the derivation of the effective lattice model to include multiple internal states (e.g., rotational or hyperfine). We end with an outlook to future research.

DOI: 10.1103/PhysRevA.95.043635

I. INTRODUCTION

Even though ultracold molecules have long been studied for their connections to quantum information [1], chemistry [2–8], and many-body physics [9–13], only recently has it been realized that nonreactive molecules (NRMs) in an optical lattice are described by an effective lattice model that is qualitatively modified from the conventional Hubbard model that governs their atomic counterparts [14]. The underlying physics is that when two molecules are close, there are many more configurations available than for two atoms: They can rotate and vibrate in many ways as they scatter off one other [15,16]. These complex rotations and vibrations can alternatively be viewed in terms of bound eigenstates, the bimolecular collisional complexes (BCCs). Reference [14] derived the form of the multichannel Hubbard model that governs ultracold NRMs in a lattice and estimated its parameters under a suite of approximations for the molecular scattering that were introduced by Refs. [15,16]. This model introduces both a multichannel on-site interaction and a channel-dependent tunneling for two molecules to reach the same site, as shown schematically in Fig. 1.

A major consequence of Ref. [14] is that all of the substantial literature that has studied NRMs in an optical lattice [10,17–22] must be reconsidered in light of the modified on-site interaction: Rather than simply augmenting the normal on-site interaction (i.e., Hubbard U) with a dipolar interaction (for polar molecules), as has been done in the previous literature, a proper treatment must also include the multichannel interaction. This on-site interaction term is not merely a small correction, but instead can potentially modify qualitative features of the physics such as the many-body phase diagram. It remains to be seen when and to what extent the modifications are significant, but we expect the effects to be substantial in many cases.

The present work is dedicated to a detailed derivation of the multichannel lattice model of Ref. [14], including generalizing this model to multiple internal states, e.g., hyperfine or rotational states. Section II presents a broad view of the past and current work in ultracold molecules, including NRMs, with special focus on optical lattice settings. This section also presents the many-body lattice model (2), the microscopic derivation of which is our main result, along with a description of the terms appearing in it. Further, this section briefly overviews few- and many-channel models in harmonic traps, which play a central role in our derivation. Readers who are not interested in this background can skip to Sec. III.

Section III derives the effective resonance model, Eq. (6) below, that governs two molecules on a single site of an optical lattice, where the two molecules couple to a dense collection of BCCs. This is a key result that is later used to obtain the lattice model, in Sec. V. In contrast to Ref. [14], which posits the form of Eq. (6), in Sec. III we provide a formal derivation from a microscopic Hamiltonian that treats the two molecules as four pairwise interacting atoms. Although this four-body problem is not straightforwardly solvable, even by advanced numerical methods, this section sets up a formalism that might allow these couplings to be computed with more advanced methods or future computational resources. It is also illuminating to see the relationship between the effective interaction parameters and conceptually simple microscopic expressions.

*Present address: Johns Hopkins University Applied Physics Laboratory, Laurel, MD 20723, USA.

†kaden.hazzard@gmail.com

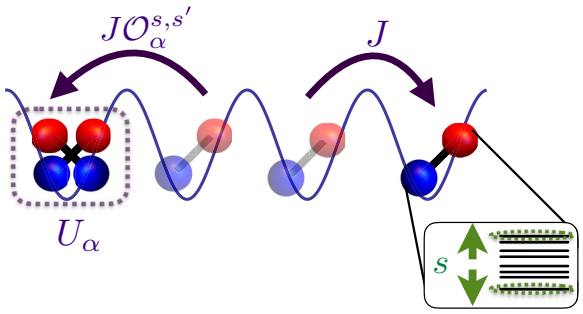

FIG. 1. Schematic of effective model (2). Ultracold NRMs in open-channel internal states s tunnel through the lattice at a rate J when moving to an empty site. When an NRM tunnels onto an occupied site, the tunneling is reduced by the open-channel weight $\mathcal{O}_\alpha^{s,s'}$, the matrix element of two open-channel molecules on the two-body on-site eigenstates $|\alpha\rangle$. Energy shifts due to collisional resonances for two NRMs on a site are described by interaction energies U_α.

As is well known from the two-channel case, the energies in resonance models diverge as the coupling of open and closed channels approaches zero range. Section IV derives in detail the regularization of the coupling constants that is necessitated to obtain finite physical results when taking the couplings to zero range. The form of this regularization has some unique features that are absent in the usual single- or two-channel cases, requiring the introduction of couplings between the bound states. Then Sec. V derives in detail the lattice model from the one-site two-particle solution. We also derive extensions of the model to multiple internal states: hyperfine, rotational, or vibrational. Finally, Sec. VI summarizes and provides an outlook.

II. OVERVIEW OF NONREACTIVE MOLECULES IN AN OPTICAL LATTICE

Atomic physics has been transformed by the development of laser cooling, which uses closed cycling transitions to remove entropy from atoms via spontaneous emission. Extending this technology directly to molecules is highly desirable, but early analyses [23] identified a limitation that persists to this day: Due to the complex internal structure of molecular rotations and vibrations, excitation energy in a molecule can be distributed through many different pathways, rendering the existence of closed cycling transitions rare. In atoms, the problem of hyperfine branching can be solved by adding repumping lasers. However, even for simple molecules, the number of lasers required makes this solution unsustainable aside from a few exceptional cases [24–30].

While direct cooling of molecules has proven to be challenging, many experiments have had success creating ultracold molecules via indirect methods. Most prominently, there has been spectacular progress in "assembling" ultracold molecules from a dual-species gas of precooled alkali-metal atoms. Here the assembly occurs in two steps. First, one associates the atoms into a loosely bound Feshbach molecule by sweeping through a magnetically tunable Feshbach resonance. Next, one coherently transfers the molecular population to the rovibrational ground state using stimulated Raman adiabatic passage [31]. This final step is possible because of modern highly coherent laser technology. The first near-degenerate gas of molecules produced in the fashion was KRb [32].

It was quickly learned that KRb, like half of the alkali-metal dimers [33], is chemically reactive through the pathway $AB + AB \rightarrow A_2 + B_2$ [34]. Since this initial demonstration, ultracold KRb molecules have enabled many fascinating studies [35–37], including phenomena such as cold collisions [34,38], suppression of chemical losses through trapping geometry [39], and the quantum Zeno effect [40], and many-body physics for which chemical reactions are irrelevant, such as quantum spin models [11,41,42].

Similar indirect molecule-production experiments have been successfully performed for the molecules RbCs [43–48], NaK [49–52], and NaRb [53,54]. Unlike KRb, these are expected to be nonreactive. In addition to the myriad experiments progressing with chemically reactive species [55–58], many experiments are under way attempting to cool molecules whose chemical reactivity is unknown [25–29,59–64]. Further details on the production of ultracold molecules through both direct and indirect means can be found in recent review articles [2,9,65–69].

The efficiency of the molecule formation process by way of magneto- or photoassociation can be enhanced relative to free space by assembling the atoms into molecules in an optical lattice, where, ideally, exactly one atom of each species that is being combined would occupy a single lattice site [70–72]. Indeed, such an enhancement in the phase-space density of KRb molecules by assembling in an optical lattice has been recently observed [73]. Hence, optical lattices are a natural setting for high-density gases of ultracold molecules, including NRMs, in near-term experiments. Not only are these systems cold, but the internal degrees of freedom can be controlled: Once in the rovibrational ground state, further transfer to any desired hyperfine state, including the absolute ground state, can then be achieved with microwave control, owing to the mixing of hyperfine and rotational angular momenta by a nuclear quadrupole coupling [48,74,75]. The use of an optical lattice is also arguably essential for many-body physics with reactive molecules; experiments must confine the molecules in particular geometries where chemical reactions are suppressed [76–78] and work at times short compared to time scales of residual losses.

In contrast to reactive molecules, NRMs do not suffer from geometrical and lifetime constraints and so lead to exciting new possibilities for many-body physics in which translational motion of the molecules and the dipole-dipole interaction both are important. Further, the possibility of having a large ratio of elastic to inelastic collisions leads to the possibility of evaporative cooling [59,79] to bring molecules even deeper into the deep ultracold regime. In order to harness these advantages of NRMs, however, we must understand the short-range collisional properties of NRMs and their implications for many-body lattice models.

Recently, it has been argued that ultracold collisions between NRMs are qualitatively different from those of alkali-metal atoms due to a remarkably high density of internal states ρ_b, i.e., rovibrational configurations, for the two-molecule system occurring at small intermolecular separations [15,16,80]

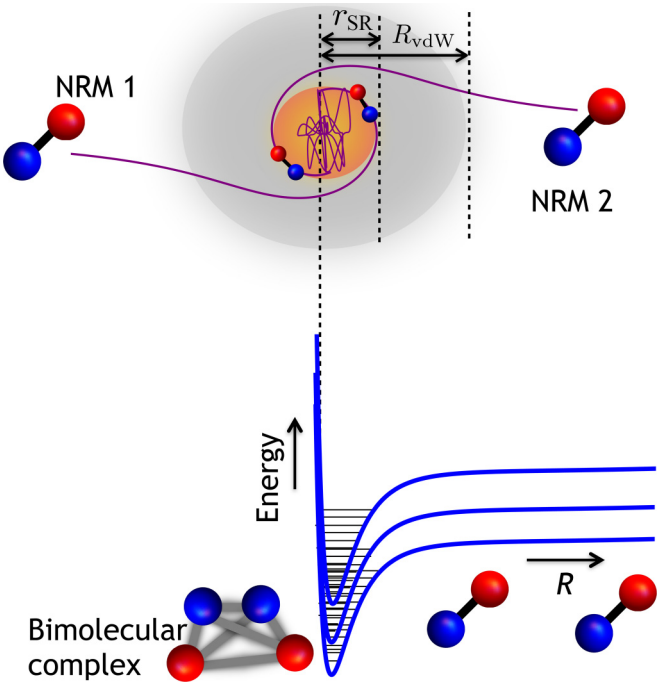

FIG. 2. Complex scattering of ultracold nonreactive molecules. At intermolecular separations large compared to a characteristic potential range R_{vdW}, molecules propagate ballistically. These ballistic trajectories are curved in a regular fashion in an intermediate range comparable to the potential length but still larger than a characteristic short-range length r_{sr}. Below r_{sr}, many internal molecular states (e.g., rotations and vibrations) become strongly mixed as the constituent atoms undergo chaotic dynamics. These complex dynamics can be recast in terms of a resonance model with a large density of rovibrational resonances [see Eq. (6)].

(see Fig. 2). A typical value is

$$\rho_b \sim \frac{1}{2\text{ nK}} \sim \frac{1}{2\pi \times 20\text{ Hz}} \quad \text{for NaK} \tag{1}$$

such that there are numerous scattering resonances within a typical thermal energy window even for the coldest $\gtrsim$100 nK NRMs. (Note that $\hbar = k_B = 1$ unless otherwise specified throughout.) These internal states lead to a near continuum of resonances that will remain unresolved for realistic experimental temperatures, in contrast to atomic collisions, in which one or at most a few resonances are relevant at ultralow collision energies. As a consequence, the standard approach for deriving effective lattice models for atoms based on a single-channel pseudopotential [81,82] will rarely apply to NRMs.

An effective model for NRMs based on this picture of a high density of resonances at zero energy was first presented in Ref. [14]. In contrast to the Hubbard model, which typically provides an accurate description for ultracold atoms in optical lattices, the effective model for NRMs takes the form of a multichannel resonance model

$$\hat{H} = -J \sum_{\langle i,j\rangle,s} [\hat{c}^\dagger_{i,s}\hat{c}_{j,s} + \text{H.c.}] + \sum_i \left(\sum_\alpha U_\alpha \hat{n}_{i,\alpha} + \frac{3\omega}{2}\hat{n}_i \right), \tag{2}$$

whose derivation is outlined below and presented in detail in Sec. V. This model, which generalizes the results of Ref. [14] to multiple open-channel states, is valid for bosonic or fermionic NRMs in a deep lattice, subject to the constraint that no more than two NRMs occupy a single lattice site. Here J is the tunneling, U_α is the interaction energy of a pair of NRMs in the state $|\alpha\rangle$, and ω is the harmonic trapping frequency of an NRM within an individual lattice site (see visualization in Fig. 1). The states $|\alpha\rangle$ are the eigenstates of the relative coordinate Hamiltonian for two particles on one site [given by Eq. (6) below]. The interaction energy U_α is found from the eigenenergy E_α of the state $|\alpha\rangle$ by $U_\alpha = E_\alpha - 3\omega/2$. The index s runs over the allowed states in the open channel, $\hat{n}_i$ counts the total number of NRMs on lattice site i, and $\hat{n}_{i,\alpha}$ measures the occupation probability of eigenstate $|\alpha\rangle$ on site i, respectively. As an example, if NRMs can be in two states (say, rotational or hyperfine) on different lattice sites, $s \in \{\uparrow,\downarrow\}$. This is controlled independently from the inevitable numerous rotational excitations of the BCC that contribute when two NRMs are on a single site and which are indexed by α. In Ref. [14], statistical distributions for the parameters appearing in this model, e.g., U_α, were identified within a series of additional approximations. A critical assay of these approximations, their possible breakdown, and more general theories are presented in the following paper [83].

The operators $\hat{c}_{i,s}$ are bosonic or fermionic operators for bosonic or fermionic NRMs, i.e., satisfy the usual (anti)commutation relations between operators on different sites, but are modified from the usual annihilation operators to account for the many interaction channels and the low-filling constraint. Explicitly, the actions of $\hat{c}^\dagger_{i,s}$ on the vacuum state $|0\rangle_i$, a lattice site with a single molecule in state $|s'\rangle_i$, and a site with two molecules in the relative state $|\alpha\rangle_i$ are

$$\hat{c}^\dagger_{i,s}|0\rangle_i = |s\rangle_i, \tag{3}$$

$$\hat{c}^\dagger_{i,s}|s'\rangle_i = P_{s,s'}\sqrt{1+\delta_{s,s'}}\sum_\alpha \mathcal{O}^{s,s'}_\alpha |\alpha\rangle_i, \tag{4}$$

$$\hat{c}^\dagger_{i,s}|\alpha\rangle_i = 0. \tag{5}$$

Equation (3) is the usual creation of a molecule on an empty site and Eq. (5) is the low-filling constraint. Equation (4) is the creation of a superposition of two-body eigenstates $|\alpha\rangle_i$ by adding a molecule to an already occupied site. The square-root term accounts for Bose stimulation when the two molecules are bosonic and in the same internal state and the coefficients $P_{s,s'}$ account for fermionic exchange and Pauli blocking (or are all unity in the case of bosons). See Sec. V for details. Finally, the overlap $\mathcal{O}^{s,s'}_\alpha \equiv \langle\alpha|s,s'\rangle$ describes the projection of two open-channel molecules on a single site i onto the set of two-body relative eigenstates $|\alpha\rangle_i$. We stress that Eq. (2) makes no assumptions about the character of the states $|\alpha\rangle_i$, for example, about the degree of lattice band mixing, provided that all energy scales (e.g., temperature and interactions U_α) are small compared to the band gap. While the definition of $\hat{c}_{i,s}$ above implies a projection from open-channel one-molecule states onto two-molecule states, such a sudden projection only occurs physically in the limit in which the tunneling is large compared to the interactions. In the opposite limit of weak tunneling compared to interactions, the uncoupled

one-molecule states on neighboring sites either evolve into an interacting state near resonance with the open channel or avoid the two-molecule sector altogether when all interacting states are off-resonance. The above definition of the operators $\hat{c}_{i,s}$ correctly captures both limits of the effective model.

The s in Eq. (2) that labels internal states in principle can refer to hyperfine, rotational, or vibrational states. It can be readily generalized to other excitations, e.g., band excitations, by making J state dependent. Two conditions are required on internal states for this model to apply. First, they must be long lived on the time scales of the experiment (ruling out extremely highly excited rotational states, moderately excited vibrational states, and nearly all electronic states). Second, the energies of the internal states must be large compared to J and U_α: This ensures that the population of each internal component is separately preserved by forcing population changing interactions to be far off-resonance. These conditions are satisfied for hyperfine levels at the $\sim$100 G magnetic fields used for magnetoassociation of atoms into molecules.

Most of these conditions are also easily satisfied for internal levels that correspond to low-lying rotational excitations of the molecules and the form of Eq. (2) remains valid. However, in this case, molecules in different rotational states on different sites can exchange rotational quanta through the dipole-dipole interaction and such "state swapping" needs to be included in Eq. (2). Also, in the presence of an electric field, for polar molecules one must add long-range $1/R^3$ interactions sites separated by distance R [17–22]. The statistical probability distributions derived for the Hamiltonian parameters in Ref. [14] must be modified when higher rotational states are considered [83].

The lattice Hamiltonian in Eq. (2) for the deep lattice is derived in two steps. First one computes the eigenstates for one and two molecules in a single lattice site, approximated by an isotropic harmonic trap $V(r) = \frac{1}{2}m\omega^2 r^2$, where r is the displacement of the molecule from the trap center and m the molecular mass. The sites are then stitched together to determine the effective lattice model. Section V describes this procedure. For the single-site system, the one-molecule solutions are the usual harmonic-oscillator wave functions and energies. The two-molecule wave functions are solutions to the Hamiltonian $\hat{H} = \hat{H}_{\text{c.m.}} + \hat{H}_{\text{rel}}$, which separates into center-of-mass and relative coordinates for the harmonic trap. Here $\hat{H}_{\text{c.m.}} = \sum_{n_{\text{c.m.}},\ell_{\text{c.m.}}} (2n_{\text{c.m.}} + \ell_{\text{c.m.}} + 3/2)\omega \, |n_{\text{c.m.}},\ell_{\text{c.m.}}\rangle \langle n_{\text{c.m.}},\ell_{\text{c.m.}}|$, where $n_{\text{c.m.}}$ and $\ell_{\text{c.m.}}$ are the principal and angular momentum numbers and $|n_{\text{c.m.}},\ell_{\text{c.m.}}\rangle$ is the corresponding center-of-mass eigenstate. The (s-wave) relative coordinate Hamiltonian of two molecules in a harmonic trap can be written as

$$\hat{H}_{\text{rel}} = \sum_n \epsilon_n \, |n\rangle \langle n| + \sum_b \nu_b \, |b\rangle \langle b| + \sum_{nb} (W_{nb} \, |n\rangle \langle b| + \text{H.c.}), \tag{6}$$

with $\epsilon_n = (2n + 3/2)\omega$. The $|b\rangle$ are the short-range BCC bound states of the system and the $|n\rangle$ are harmonic-oscillator states. Under the assumption that the oscillator length $l_{\text{HO}} = \sqrt{1/\mu\omega}$, with $\mu = m/2$ the reduced mass (for two molecules, each of mass m), is large compared to the microscopic lengths that characterize the intermolecular interactions, the couplings simplify to

$$W_{nb} = w_b M_n / l_{\text{HO}}^{3/2} \tag{7}$$

for some set of w_b that depends only on the BCC properties and with

$$M_n = \sqrt{\frac{\Gamma(n + 3/2)}{\Gamma(n + 1)}}, \tag{8}$$

where $\Gamma(x)$ is Euler's Gamma function. An exact (though formal) derivation of this is discussed in Sec. III.

One could calculate the ν_b and w_b and from these calculate the U_α and $\mathcal{O}_\alpha^{s,s'}$ without approximation if one had highly accurate multichannel interatomic interaction potentials between the atoms constituting the molecules. Even with such potentials, the resulting numerical calculation would be formidable. Although we will not solve the resulting equations, Sec. III formally sets up the equations necessary to carry out this procedure in principle. Furthermore, even without solving it, it allows us to identify that the *form* of the effective model (2) is in principle exact and robust beyond the approximations used in Ref. [14]. In addition to providing the foundation for future work, it serves to clarify the meaning of the ν_b and w_b.

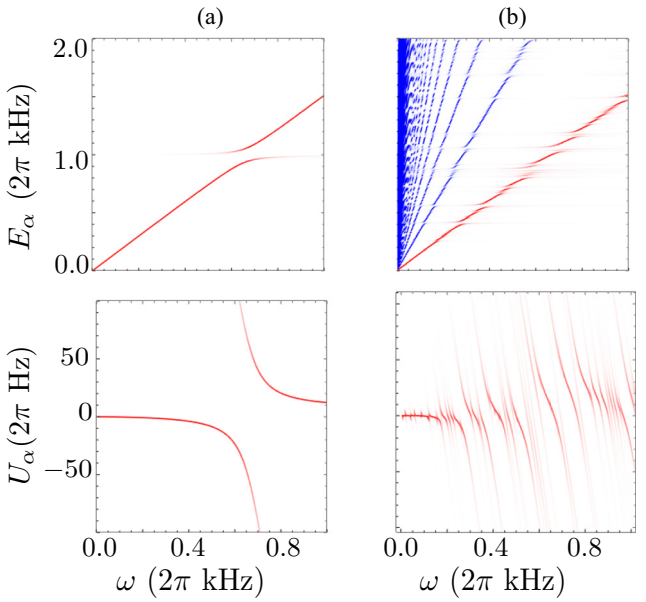

FIG. 3. Eigenvalues E_α (top row) and effective interactions U_α (bottom row) as a function of trap frequency ω. (a) Generic structure illustrated by a two-channel (single-bound-state) model. Shown on top is the relative coordinate eigenenergy E_α showing an avoided crossing between a bimolecular collisional complex at fixed energy $2\pi \times 1.0$ kHz and the harmonic-oscillator ground state that is linearly dependent on ω (diagonal). The opacity at each plotted point (darkness of the line) is set to be $\mathcal{O}_\alpha$ of the corresponding eigenstate, indicating its importance to the lattice model. Shown on bottom is the on-site interaction in the lowest band (harmonic-oscillator ground state) U_α. The avoided crossing in E_α manifests as a strong multivalued interaction near the crossing. Also shown are (b) E_α (top) and U_α (bottom) for realistic parameters for RbCs. Isolated resonances at small ω give way to coupled resonances at larger ω.

Figure 3 shows the eigenvalues E_α of Eq. (6) and the lattice model parameters $\mathcal{O}_\alpha \equiv \mathcal{O}_\alpha^{1,1}$ and U_α as a function of ω for a toy model with a single BCC [Fig. 3(a)] and for an NRM with realistic properties [Figs. 3(a) and 3(b)] (estimated for the bosonic NRM RbCs), as determined by the statistical framework of Ref. [14]. Although the precise form of the results depends on the details of the approximations of this statistical framework, the qualitative structure is expected to be robust against these approximations.

Figure 3(a) shows the building block that is key to understanding all of the relevant structure seen in the model parameters. It shows results for a two-channel model, i.e., a model with a single bound state, and focuses on the ground harmonic-oscillator state. Because the bound state is so tightly confined, its relative-coordinate energy is independent of the trap and hence ω. Absent coupling to the open channels (i.e., for $W_{nb} = 0$), it would form a horizontal line, whose value in Fig. 3(a) is chosen to be $2\pi \times 1.0$ kHz for illustration. The harmonic-oscillator relative-coordinate ground-state energy $3\omega/2$ gives the diagonal line. The coupling W_{0b} between these two states leads to the avoided crossing structure in E_α that is observed in the top panel of Fig. 3(a). The contribution of the eigenstate to the lattice model is given by its overlap $\mathcal{O}_\alpha$ with the harmonic-oscillator state. The relevant eigenstate's energy is predominantly on the diagonal line except close to the resonance. Close to the resonance both states become important until they are equally weighted at resonance. The result for U_α follows from this: The U_α is the deviation of the eigenenergy E_α from the noninteracting energy (harmonic-oscillator ground state). The U_α is close to zero for the single relevant state far from the resonance. Near the resonance, two U_α are important, with values $\pm W_{0b}/2$.

Turning to the more general case, Fig. 3(b) shows results for parameters estimated for a typical NRM RbCs. At small ω, a series of isolated resonances exists, with the behavior near each similar to the two-channel cases. At larger ω these resonances smear together.

III. MICROSCOPIC CALCULATION OF w_b AND ν_b FROM INTERATOMIC POTENTIALS

In principle, the couplings w_b and energies ν_b can be calculated from a solution to the four-atom Schrödinger equation. While such a calculation remains a technical challenge that we do not pursue here, the derivation itself helps to develop an intuitive understanding for the microscopic origin of these parameters and may some day lead to a real solution of the problem. Our goal here is twofold: first, to derive Eq. (6) from a coordinate space representation of the four-atom system and give expressions for w_b and ν_b in terms of four-atom wave functions in the adiabatic hyperspherical representation [84] and second, to justify the factorization of the coupling $W_{nb} = w_b M_n / l_{\rm HO}^{3/2}$. For simplicity, the current treatment considers only the spatial degrees of freedom associated with the atoms and quantum numbers associated with the electronic or spin degrees of freedom are suppressed. It can however be readily generalized to include atomic hyperfine structure, molecules with more than two atoms, or an even lower-level description in terms of nuclei and electrons. Readers familiar with methods in few-body physics will recognize Eqs. (9)–(16) as standard material [84–86] that is included here to provide the necessary background for what follows.

A. Derivation of the two-body Hamiltonian (6)

Our purpose here is to demonstrate how the multichannel molecule-molecule Hamiltonian (6) emerges from a four-atom ($N = 4$) problem in the limit where the intermolecular separation is large compared to the dimer size. In doing so, the molecule-molecule interaction channels become unambiguously specified and a formula for the channel couplings W_{nb} is obtained. The reduction to a multichannel model is facilitated by expressing the positions $\{\boldsymbol{r}_i\}$ of the atoms in a set of mass-scaled H-type Jacobi coordinates $\{\boldsymbol{\rho}_i\}$:

$$\begin{aligned}
\boldsymbol{\rho}_1 &= \sqrt{\frac{\mu_{1,2}}{\mu_{4\rm B}}}(\boldsymbol{r}_1 - \boldsymbol{r}_2), \quad \boldsymbol{\rho}_2 = \sqrt{\frac{\mu_{3,4}}{\mu_{4\rm B}}}(\boldsymbol{r}_3 - \boldsymbol{r}_4), \\
\boldsymbol{\rho}_3 &= \sqrt{\frac{\mu_{12,34}}{\mu_{4\rm B}}}\left(\frac{m_3\boldsymbol{r}_3 + m_4\boldsymbol{r}_4}{m_3 + m_4} - \frac{m_1\boldsymbol{r}_1 + m_2\boldsymbol{r}_2}{m_1 + m_2}\right), \\
\boldsymbol{X} &= \frac{m_1\boldsymbol{r}_1 + m_2\boldsymbol{r}_2 + m_3\boldsymbol{r}_3 + m_4\boldsymbol{r}_4}{m_1 + m_2 + m_3 + m_4}.
\end{aligned} \tag{9}$$

Here $\mu_{i,j} = m_i m_j/(m_i + m_j)$ is the reduced mass of particles (or clusters) i and j. The mass scale $\mu_{4\rm B}$ is arbitrary, but is often chosen as $\mu_{4\rm B} = (\mu_{1,2}\mu_{3,4}\mu_{12,34})^{1/3}$ in order to preserve the integration volume element [87]. Note that $\mu_{12,34}$ coincides with $\mu = m/2$ introduced in [14] and in Sec. II above. In a harmonic trapping potential, the center-of-mass motion decouples completely from the relative motion, allowing one to write $\Psi = \Psi_{\rm rel}(\boldsymbol{\rho}_1, \boldsymbol{\rho}_2, \boldsymbol{\rho}_3)\Psi_{\rm c.m.}(\boldsymbol{X})$. The remaining $d = 3N - 3 = 9$ relative coordinates may be transformed to hyperspherical coordinates $\{\boldsymbol{\rho}_1, \boldsymbol{\rho}_2, \boldsymbol{\rho}_3\} \to \{R, \Omega\}$, where R is the hyperradius, defined as

$$R^2 = \rho_1^2 + \rho_2^2 + \rho_3^2, \tag{10}$$

and Ω collectively denotes all of the eight remaining relative angular coordinates. This transformation can be made by defining canonical hyperangles, as reviewed, for example, in [88], or through the introduction of so-called democratic hyperangles [86,89–91], which are capable of treating all fragmentation channels on an equal footing. Because the hyperradius R is invariant with respect to particle permutations, it proves to be a more convenient collision coordinate than the intermolecular separation. A significant conceptual advantage afforded by this choice is that all exchange symmetry can be incorporated into the hyperangular channel functions by appropriate boundary conditions on the hypersphere, with no need for additional atom-exchange interactions in the four-atom potential energy surface. Note that if the size of each dimer is negligible in comparison to the intermolecular separation, then the hyperradius is approximately equal to the molecular separation.

The bimolecular Hamiltonian for the relative degrees of freedom in hyperspherical coordinates can then be expressed as

$$\begin{aligned}
\hat{H}_{\rm rel} = &-\frac{1}{2\mu_{4\rm B}R^{d-1}}\frac{\partial}{\partial R}\left(R^{d-1}\frac{\partial}{\partial R}\right) + \frac{1}{2}\mu_{4\rm B}\omega^2 R^2 \\
&+ \frac{\hat{\Lambda}^2(\Omega)}{2\mu_{4\rm B}R^2} + \hat{V}(R, \Omega).
\end{aligned} \tag{11}$$

Here $\hat{\Lambda}^2/2\mu_{4B}R^2$ represents the hyperangular (fixed R) kinetic energy, where $\hat{\Lambda}$ is the hyperangular momentum [92]. The harmonic-oscillator potential is purely hyperradial and $\hat{V}(R,\Omega)$ contains all interatomic interactions. The particular form of $\hat{V}(R,\Omega)$ is not important for our purpose, except that it depends only on relative degrees of freedom. We represent eigenstates $\Psi_{\rm rel}(R,\Omega)$ of $\hat{H}_{\rm rel}$ by writing

$$\Psi_{\rm rel}(R,\Omega) = \sum_\alpha F_\alpha(R)\Phi_\alpha(R;\Omega), \tag{12}$$

where the channel functions Φ_α are defined as eigenstates of the adiabatic Hamiltonian

$$\hat{H}_{\rm ad} = \frac{\Lambda^2}{2\mu_{4B}R^2} + \hat{V}(R,\Omega), \tag{13}$$

with R-dependent adiabatic potentials $\mathcal{U}_\alpha(R)$ as eigenvalues:

$$\hat{H}_{\rm ad}(R;\Omega)\Phi_\alpha(R;\Omega) = \mathcal{U}_\alpha(R)\Phi_\alpha(R;\Omega). \tag{14}$$

Inserting Eq. (12) into the eigenequation for Eq. (11) and making use of Eq. (14) leads to a set of coupled channel equations in R for F_α,

$$\sum_\beta \Bigg[\left(-\frac{1}{2\mu_{4B}}\frac{d^2}{dR^2} + \frac{1}{2}\mu_{4B}\omega^2R^2 + \mathcal{U}_\alpha^{\rm eff}(R) - E\right)\delta_{\alpha\beta} - \frac{1}{2\mu_{4B}}\left(2P_{\alpha\beta}(R)\frac{d}{dR} + (1-\delta_{\alpha\beta})Q_{\alpha\beta}(R)\right)\Bigg] \times R^{(d-1)/2}F_\beta(R) = 0. \tag{15}$$

The factor of $R^{(d-1)/2}$ is present to facilitate the removal of first-derivative terms in the radial kinetic energy. The effective potential in each channel becomes

$$\mathcal{U}_\alpha^{\rm eff}(R) = \mathcal{U}_\alpha(R) - \frac{Q_{\alpha\alpha}(R)}{2\mu_{4B}} + \frac{(d-1)(d-3)/4}{2\mu_{4B}R^2}. \tag{16}$$

It is critical to include the positive diagonal contribution $-Q_{\alpha\alpha}(R)/2\mu_{4B}$ in order to obtain the correct large-R behavior of $\mathcal{U}_\alpha^{\rm eff}$, which must approach the binding energy of two separated NRMs in their rovibrational ground state. The channels are coupled by nonadiabatic first-derivative and second-derivative couplings, defined as

$$P_{\alpha\beta}(R) = \left\langle \Phi_\alpha \middle| \frac{\partial\Phi_\beta}{\partial R}\right\rangle, \quad Q_{\alpha\beta}(R) = \left\langle \Phi_\alpha \middle| \frac{\partial^2\Phi_\beta}{\partial R^2}\right\rangle, \tag{17}$$

where the integration in these matrix elements is carried out over angular coordinates only. Because the channel functions are orthonormal at each R, $\frac{\partial}{\partial R}\langle\Phi_\alpha|\Phi_\beta\rangle = 0$ immediately gives that $P_{\alpha\beta}$ is antisymmetric and thus zero along the diagonal. The functions $F_\alpha(R)$ can be expanded in a complete set of states ψ_α^i for each α as

$$R^{(d-1)/2}F_\alpha(R) = \sum_i R\psi_\alpha^i(R). \tag{18}$$

It is then straightforward to show that the Hamiltonian operator $\hat{H}_{\rm rel}$ can be written in the form

$$\hat{H}_{\rm rel} = \sum_{\alpha,i}\sum_{\beta,j}\left|\psi_\alpha^i\alpha\right\rangle\left(\delta_{\alpha\beta}\mathcal{H}_{\beta\beta}^{ij} + \mathcal{X}_{\alpha\beta}^{ij}\right)\left\langle\psi_\beta^j\beta\right|, \tag{19}$$

where we define the diagonal matrix element $\mathcal{H}_{\beta\beta}^{ij}$,

$$\mathcal{H}_{\beta\beta}^{ij} = \int_0^{R_m}\left[\frac{1}{2\mu_{4B}}\frac{d\psi_\beta^i}{dR}\frac{d\psi_\beta^j}{dR} + \psi_\beta^i\left(\mathcal{U}_\beta^{\rm eff}(R) + \frac{1}{2}\mu_{4B}\omega^2R^2\right)\psi_\beta^j\right]R^2dR, \tag{20}$$

and the channel coupling matrix elements as

$$\mathcal{X}_{\alpha\beta}^{ij} = -\frac{1}{2\mu_{4B}}\int_0^{R_m}\left[P_{\alpha\beta}(R)\left(\psi_\alpha^i\frac{d\psi_\beta^j}{dR} - \psi_\beta^j\frac{d\psi_\alpha^i}{dR}\right) - (1-\delta_{\alpha\beta})\psi_\alpha^i\psi_\beta^j\tilde{Q}_{\alpha\beta}(R)\right]R^2dR. \tag{21}$$

In order to demonstrate that $\hat{H}_{\rm rel}$ is explicitly symmetric, we have introduced the symmetric form of the second derivative coupling

$$\tilde{Q}_{\alpha\beta}(R) = \left\langle\frac{\partial\Phi_\alpha}{\partial R}\middle|\frac{\partial\Phi_\beta}{\partial R}\right\rangle, \tag{22}$$

which is related to the matrices P and Q by $\tilde{Q} = \frac{\partial P}{\partial R} - Q$.

Ultimately, to derive Eq. (6), a rigorous connection between the $(d=9)$-dimensional four-atom space and the effectively three-dimensional (3D) molecule-molecule channel is needed. To enable such a connection, we first focus on the solutions to Eq. (15) ignoring all off-diagonal elements $\alpha \neq \beta$, which we denote by $f_\alpha(R)$. First, we write $\mathcal{U}_\alpha(R) - Q_{\alpha\alpha}(R)/2\mu_{4B} = \lambda(\lambda+d-2)/2\mu_{4B}R^2$, where λ is assumed to be in general a function of R and independent of R only for the noninteracting case where it is equal to the hyperangular momentum eigenvalue of the $\hat{\Lambda}^2$ operator [92]. It is convenient to define an "effective" hyperangular momentum $\ell_{\rm eff} = \lambda + (d-3)/2$ such that the uncoupled radial function $f_\alpha(R)$ satisfies

$$\left[-\frac{1}{2\mu_{4B}}\frac{d^2}{dR^2} + \frac{1}{2}\mu_{4B}\omega^2R^2 + \frac{(\ell_{\rm eff}+1/2)^2 - 1/4}{2\mu_{4B}R^2} - E\right] \times R^{(d-1)/2}f_\alpha(R) = 0. \tag{23}$$

The solution for *constant* $\ell_{\rm eff}$ is [93]

$$\tilde{R}^{(d-1)/2}f_{n,\ell_{\rm eff}}(\tilde{R}) = \sqrt{\frac{2n!}{\Gamma\left(n+\frac{3}{2}\right)}}\tilde{R}^{\ell_{\rm eff}+1}e^{-\tilde{R}^2/2}L_n^{\ell_{\rm eff}+1/2}(\tilde{R}^2), \tag{24}$$

where $\tilde{R} = R/\sqrt{1/\mu_{4B}\omega}$. For s-wave scattering in any of the two-body channels, we expect that as $R \gg R_{\rm vdW}$, $[(\ell_{\rm eff}+1/2)^2 - 1/4]/2\mu_{4B}R^2 \to E_{\rm mm}$, where $E_{\rm mm}$ is the threshold energy of the molecule-molecule channel. Thus, Eq. (23) for constant $\ell_{\rm eff}$ is reduced to an s-wave harmonic-oscillator equation whose solutions, Eq. (24), have eigenvalues $E_n = E_{\rm mm} + \omega(2n+3/2)$ and are simply related to the 3D s-wave oscillator eigenfunctions ψ_ℓ^n by $R^{(d-1)/2}f_{n,\ell_{\rm eff}=0}(R) = R\psi_{\ell=0}^n(R)$. These oscillator functions are precisely the basis functions chosen to represent the open-channel wave-function component. They are eigenstates of the open-channel problem in the absence of coupling to bound states and in the absence of an open-channel resonance. It is convenient to measure their

eigenenergy with respect to the molecule-molecule threshold by writing

$$\epsilon_n = E_n - E_{\rm mm} = \omega(2n + 3/2). \tag{25}$$

To proceed, let O denote the open channel and B denote a closed channel. The open-channel s-wave oscillator basis states described above are now denoted by $|\psi_O^n\rangle$. Basis states in each closed channel are chosen to be the set of bound eigenstates $|\psi_B^a\rangle$ of the single-channel Hamiltonian $\hat{H}_B = \sum_{i,j} |\psi_B^i B\rangle \mathcal{H}_{BB}^{ij} \langle \psi_B^j B|$ with eigenvalue λ_B^a. That is, we let

$$|\psi_\alpha^j \alpha\rangle = \begin{cases} |\psi_B^a B\rangle, & \alpha \in B \\ |\psi_O^n O\rangle, & \alpha \in O, \end{cases} \tag{26}$$

where $\hat{H}_B|\psi_B^a\rangle = \lambda_B^a|\psi_B^a\rangle$. The states $|\psi_O^n\rangle$ would have difficulty capturing the short-range boundary condition in the presence of a shallow bound state in the open channel. In that case, one could alternatively use the known solutions for a contact interaction in a harmonic trap [94].

With only one open channel, the Hamiltonian can be written explicitly in terms of open and bound channels as

$$\begin{aligned} \hat{H}_{\rm rel} = &\sum_n |\psi_O^n O\rangle \epsilon_n \langle \psi_O^n O| + \sum_{Ba} |\psi_B^a B\rangle \lambda_B^a \langle \psi_B^a B| \\ &+ \sum_n \sum_{B,a} \left(|\psi_O^n O\rangle \mathcal{X}_{OB}^{na} \langle \psi_B^a B| + \text{H.c.} \right) \\ &+ \sum_{B,B',a,a'} |\psi_B^a B\rangle \mathcal{X}_{BB'}^{aa} \langle \psi_{B'}^{a'} B'|. \end{aligned} \tag{27}$$

Equation (27) defines the various matrix elements in terms of open- and closed-channel basis states. The states $|b\rangle$ appearing in Eq. (6) are obtained by diagonalizing the subspace of bound-bound channels $\hat{H}_{\rm b}|b\rangle = \nu_b|b\rangle$, where

$$\hat{H}_{\rm b} = \sum_{aB} |\psi_B^a B\rangle \lambda_B^a \langle \psi_B^a B| + \sum_{B,B',a,a'} |\psi_B^a B\rangle \mathcal{X}_{BB'}^{aa'} \langle \psi_{B'}^{a'} B'|. \tag{28}$$

One can write the resulting eigenstates as $|b\rangle = \sum_{aB} \langle \psi_B^a B|b\rangle |\psi_B^a B\rangle$. Rotating into the basis of eigenstates of $\hat{H}_{\rm b}$, the block structure of the Hamiltonian becomes

$$\begin{aligned} \hat{H}_{\rm rel} &= \left(\begin{array}{c|ccc} OO & OB_1 & OB_2 & \cdots \\ \hline B_1O & B_1B_1 & B_1B_2 & \cdots \\ B_2O & B_2B_1 & B_2B_2 & \cdots \\ \vdots & \vdots & \vdots & \ddots \end{array}\right) \\ &\to \left(\begin{array}{c|ccc} \epsilon_n & \cdots & W_{nb} & \cdots \\ \hline \vdots & \ddots & 0 & 0 \\ W_{bn} & 0 & \nu_b & 0 \\ \vdots & 0 & 0 & \ddots \end{array}\right). \end{aligned} \tag{29}$$

The energies ν_b and the couplings W_{nb} are now given explicitly in terms of the eigenstates of the microscopic Schrödinger equation as

$$\nu_b = \sum_{B,B',a,a'} \langle b|\psi_B^a B\rangle \langle \psi_{B'}^{a'} B'|b\rangle \left(\lambda_B^a \delta_{aB,a'B'} + \mathcal{X}_{BB'}^{aa'}\right), \tag{30}$$

$$W_{nb} = \sum_{B,a} \langle \psi_B^a B|b\rangle \mathcal{X}_{OB}^{na} \tag{31}$$

such that with the shorthand $|n\rangle = |\psi_O^n O\rangle$, we recover Eq. (6),

$$\begin{aligned} \hat{H}_{\rm rel} = &\sum_{n,b} (|n\rangle W_{nb} \langle b| + \text{H.c.}) \\ &+ \sum_b |b\rangle \nu_b \langle b| + \sum_n |n\rangle \epsilon_n \langle n|. \end{aligned} \tag{32}$$

B. Factorization of W_{nb}

Finally, we sketch how the separation of length scales $l_b \ll l_{\rm HO}$, with l_b the characteristic length scale of the bound state, allows for the factorization of $W_{nb} = w_b M_n / l_{\rm HO}^{3/2}$. We focus on the channel coupling elements between the open and closed channels,

$$\begin{aligned} \mathcal{X}_{OB}^{na} = -\frac{1}{2\mu_{\rm 4B}} \int_0^{R_m} &\left[P_{OB} \left(\psi_O^n \frac{d\psi_B^a}{dR} - \psi_B^a \frac{d\psi_O^n}{dR} \right) \right. \\ &\left. - \tilde{Q}_{OB} \psi_O^n \psi_B^a \right] R^2 dR. \end{aligned} \tag{33}$$

The closed-channel eigenfunctions ψ_B^a are all short range with support only over length scales $R \sim l_b$ and exponentially small for $R \gtrsim l_b$. On the other hand, the oscillator state $\psi_O^n(R)$ is a long-range function that varies over length $l_{\rm HO}/\sqrt{n}$.

In order to exploit this separation of length scales, we first note that at short range, we may approximate the slowly varying oscillator state as $\psi_O^n(R) \approx \psi_O^n(0) + [\frac{d\psi_O^n}{dR}]_0 R$. Using Eq. (24) with $\ell_{\rm eff} = 0$, along with the fact that we have chosen our open-channel basis functions to be $R\psi_O^n = R^{(d-1)/2} f_{n,\ell_{\rm eff}=0}$, we find

$$\psi_O^n(0) = \sqrt{\frac{8\Gamma(n+3/2)}{l_{\rm HO}^3 \pi\ \Gamma(n+1)}}, \quad \left[\frac{\partial \psi_O^n}{\partial R}\right]_{R=0} = 0. \tag{34}$$

Because $\psi_B^a(R)$ has support only for $R \sim l_b$, the term in Eq. (33) containing $\frac{\partial \psi_O^n}{\partial R}$ is negligible compared to the other terms and Eq. (33) is cast into the form

$$\mathcal{X}_{OB}^{na} = -\frac{1}{2\mu_{\rm 4B}} \psi_O^n(0) \int_0^{R_m} \mathcal{I}_{OB}^a(R) R^2 dR, \tag{35}$$

where we have defined

$$\mathcal{I}_{OB}^a(R) = P_{OB}(R) \left(\frac{d}{dR} - \tilde{Q}_{OB}(R) \right) \psi_B^a(R). \tag{36}$$

Alternatively, one could perform an integration by parts on the second term in Eq. (33), removing the derivative on ψ_O^n. The resulting surface term vanishes, and using the relation $\tilde{Q} = \frac{\partial P}{\partial R} - Q$, one obtains an equivalent expression for $\mathcal{I}_{OB}^a$,

$$\mathcal{I}_{OB}^a(R) = \left[2P_{OB}(R) \left(\frac{d}{dR} + \frac{1}{R} \right) + Q_{OB}(R) \right] \psi_B^a(R). \tag{37}$$

The function $\mathcal{I}^a_{OB}(R)$ has support only at length scales $R \sim l_b$. Finally, the couplings W_{nb} given in Eq. (31) are written as

$$W_{nb} \approx -\frac{\psi^n_O(0)}{2\mu_{4B}} \sum_{B,a} \langle \psi^a_B B | b \rangle \int_0^{R_m} \mathcal{I}^a_{OB}(R) R^2 dR. \quad (38)$$

Using Eq. (34), one recovers Eqs. (7) and (8) such that the couplings w_b are now given as

$$w_b = -\frac{\sqrt{2}}{\sqrt{\pi}\mu_{4B}} \sum_{B,a} \langle \psi^a_B B | b \rangle \int_0^{R_m} \mathcal{I}^a_{OB}(R) R^2 dR. \quad (39)$$

Were we to include an open-channel resonance by replacing the oscillator states ψ^n_O with the known two-body solutions for zero-range interactions [94], then the ϵ_n and M_n would be shifted, but the w_b, which are independent of open-channel states, would be unchanged.

To summarize, in order to determine the energies ν_b, one would first calculate the adiabatic channel functions $\Phi_\alpha(R;\Omega)$ and potentials $\mathcal{U}_\alpha(R)$ by solving the eigenvalue problem (14) and then calculate the nonadiabatic couplings $P_{\alpha\beta}(R)$ and $\tilde{Q}_{\alpha\beta}(R)$ by Eqs. (17) and (22). One could then calculate the couplings $\mathcal{X}^{ij}_{\alpha\beta}$ by performing the integrals in Eq. (21) before finally diagonalizing $\hat{H}_b$ given in Eq. (28) to find its eigenvalues ν_b. Diagonalizing Eq. (28) also yields the overlaps $\langle \psi^a_B B | b \rangle$ that appear both in Eq. (31) for the couplings W_{nb} and in Eq. (39) for the factorized coupling w_b. In this way, all of the parameters in the zero-range model (6) may in principle be determined from a microscopic theory.

Finally, we note that the adiabatic hyperspherical representation employed above, while conceptually illuminating, suffers from some shortcomings that may make a practical calculation difficult. In practice, the hyperradial derivatives in Eq. (17) are usually estimated by a three-point difference rule. In cases where the potential curves exhibit sharp avoided crossings, the couplings are sharply peaked and difficult to calculate accurately. The method of slow variable discretization [95] (SVD) circumvents the calculation of hyperradial derivatives and has been shown to provide fast convergence for three-body systems with many two-body bound states where sharp avoided crossings are likely to appear [96–98]. Future work should include extending the current derivation to the discrete variable representation central to the SVD technique of Ref. [95].

IV. REGULARIZATION OF INTERACTIONS IN THE TWO-BODY MULTICHANNEL MODEL

Although the bound states and couplings to them in Sec. III have a finite range, since they are small compared to l_{HO} we find it convenient to work with the zero-range limit of these couplings, for example, in Eq. (7). However, fixing the bound-state energies and taking the zero-range limit is problematic and leads to divergences.

In this section we describe how Eq. (6) may be regularized to obtain the physical Hamiltonian from which the effective parameters of Eq. (2) are calculated. The naive zero-range limit takes the bound-state energies ν_b to be fixed in the absence of a coupling W_{nb} and approximates the bound-state wave functions as having zero range. This naive limit could be obtained from the results in Sec. III B by taking $l_b \to 0$, allowing us to apply Eqs. (38) and (39) for all n. However, the true physical limit is a bit more subtle: The *physical* bound-state energies are indeed some finite, fixed set of numbers, but these are not the same as the ν_b in Eq. (6). Rather, the physical energies correspond to the eigenenergies after coupling to the open channel. Analogous to the well-known one- and two-channel cases [99], this coupling to the continuum gives a divergent shift of the eigenenergies away from the ν_b. Although the regularization of the one- and two-channel models is standard and requires only a (diverging) shift in the bare bound-state energies, the regularization of a multichannel model such as ours requires new forms of couplings and the appropriate regularization is derived in Ref. [14].

Figure 4 summarizes the logic of the derivation of the regularized Hamiltonian, which we outline before giving it in detail. The basic approach is to calculate the effective low-energy Hamiltonian for the model that we claim is the proper regularized zero-range limit. Then we calculate the effective low-energy Hamiltonian for the true multichannel physical Hamiltonian, whose form and general properties we know, even though we do not know the values of the parameters appearing in it. Finally, we show that parameters for the zero-range Hamiltonian can be chosen such that its effective Hamiltonian matches the true Hamiltonian's effective Hamiltonian at low energies, thereby confirming the proposed form of the regularized Hamiltonian.

The Hamiltonian that properly accounts for the zero-range limit (as argued below) is the $\Lambda \to \infty$ limit of

$$\begin{aligned}\hat{H}_{\rm rel}(\Lambda) = &\sum_{n \text{ with } \epsilon_n < \Lambda} \epsilon_n |n\rangle \langle n| \\ &+ \sum_{b,b'} \left(\delta_{bb'} \nu^\star_b + \sqrt{\frac{\mu^3 \Lambda}{2}} w_b w_{b'} \right) |b\rangle \langle b'| \\ &+ \sum_{b,n \text{ with } \epsilon_n < \Lambda} \left(\frac{w_b M_n}{l^{3/2}_{\rm HO}} |n\rangle \langle b| + \text{H.c.} \right), \quad (40)\end{aligned}$$

where Λ is a high-energy cutoff (short-distance l_Λ cutoff) for the open channel. This energy cutoff means that the sum over harmonic-oscillator states n runs only to a value $n^\star$ such that states with $n < n^\star$ have energies $\epsilon_n < \Lambda$. Explicitly, $n^\star = \lfloor \Lambda/2\omega - 3/4 \rfloor$, although it suffices to take $n^\star = \Lambda/2\omega$ since we take the $\Lambda \to \infty$ limit. The key addition to Eq. (6) to obtain the physical zero-range limit is the term proportional to $\sqrt{\Lambda}$ that couples bound states $|b\rangle$ and $|b'\rangle$ and shifts the energy of each bound state $|b\rangle$. We now show (i) that the physical properties of Eq. (40) are independent of Λ for $\Lambda/\omega \gg 1$ [i.e., Eq. (40) is a regularization of Eq. (6)] and (ii) that Eq. (40) can reproduce the low-energy properties of the true microscopic physical Hamiltonian [i.e., it is the appropriate physical regularization].

For the first point, we want to compute $H_{\rm rel}(\Lambda)$'s effective Hamiltonian $\hat{H}_{\rm eff}(\Lambda')$ defined to act on the low-energy restricted Hilbert space that includes only bound states and open-channel states with $\epsilon_n < \Lambda'$. The effective Hamiltonian in a restricted Hilbert space may be obtained by second-order degenerate perturbation theory (i.e., a Schrieffer-Wolff

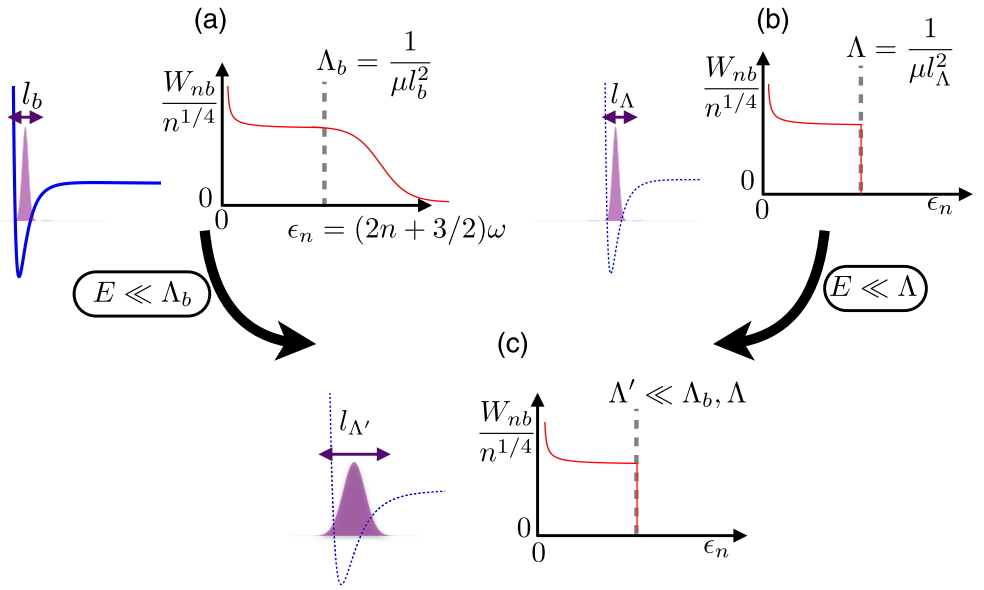

FIG. 4. Derivation of the regularized model (40). (b) The regularized zero-range limit $H_{\rm rel}$ of (a) the true physical model H_p is computed by ensuring the agreement of the forms of (c) their low-energy effective Hamiltonians $H_{\rm eff}$, which govern all of the low-energy observables. Even though the true physical Hamiltonian cannot be computed, its form can be determined [see Eq. (39)] and shown to match that obtained from the regularized model for appropriately chosen W_{nb} and ν_b.

transformation):

$$\hat{H}_{\rm eff}(\Lambda') = \hat{H}_{\rm rel}(\Lambda') - {\sum_{n,b,b'}}' \frac{w_b w_{b'} M_n^2}{\epsilon_n l_{\rm HO}^3} |b\rangle \langle b'| \qquad (41)$$

(to leading order in $1/\Lambda'$), where $\sum'$ indicates a sum over n such that $\Lambda' < \epsilon_n < \Lambda$. The second term represents the fluctuations to the high-energy Hilbert space with $\epsilon_n > \Lambda'$ that are being eliminated. It is $-\mathcal{J}\sum_{b,b'} w_b w_{b'}/l_{\rm HO}^3 |b\rangle \langle b'|$ with $\mathcal{J} = \sum_n' M_n^2/\epsilon_n$. As $\{\Lambda, \Lambda'\} \to \infty$, $\mathcal{J} \approx \sqrt{\mu^3/2l_{\rm HO}^3}(\sqrt{\Lambda} - \sqrt{\Lambda'})$. Adding this term to $\hat{H}_{\rm rel}(\Lambda')$, we see that the $\sqrt{\Lambda}$ terms cancel so that Λ in $\hat{H}_{\rm rel}$ is effectively replaced by Λ':

$$\hat{H}_{\rm eff}(\Lambda') = \hat{H}_{\rm rel}(\Lambda'). \qquad (42)$$

This is not vacuous: It says that the effective Hamiltonian for the $\epsilon_n < \Lambda'$ subspace is simply the Hamiltonian in Eq. (40) (whose $\Lambda \to \infty$ limit is used to define the theory) evaluated at the lower cutoff Λ'. This shows immediately that in contrast to the unregularized Hamiltonian in Eq. (6) the $\hat{H}_{\rm rel}(\Lambda)$ is finite: Since $\hat{H}_{\rm eff}(\Lambda')$ is defined on a space with a finite cutoff and gives identical low-energy physics as $\hat{H}_{\rm rel}$ at any value of Λ, the physics described by $\hat{H}_{\rm rel}(\Lambda)$ is Λ independent. In particular, one can take $\Lambda \to \infty$ when this is convenient.

Now we show that not only is Eq. (40) finite, it reproduces the low-energy observables of the true physical Hamiltonian H_p. Our approach will be to compute the effective low-energy Hamiltonian at energy Λ' associated with $\hat{H}_p$, which we denote by $\hat{H}_p(\Lambda')$, and match the parameters of Eq. (40) to reproduce it. We can do this without knowing the details of $\hat{H}_p$: We need merely some of its general properties. In contrast to Eq. (40), W_{nb} factors as $w_b M_n/l_{\rm HO}^{3/2}$ only for sufficiently small n that the harmonic-oscillator wave function varies slowly over the length scale of the bound state. Note that this w_b is associated with the physical Hamiltonian and not the regularized Hamiltonian; we avoid introducing new notation and the variables are to be distinguished by context. We will relate the w_b in the two models shortly.

At large n the harmonic-oscillator state probes the short-range (high-energy) physics on the scale of the bound-state size and there is no simple expression for the W_{nb}. Nevertheless, we may formally determine the Hamiltonian describing low-energy observables below a cutoff Λ' as above, as we know that the W_{nb} fall off very rapidly at some energy scale Λ_b (corresponding to a length scale l_b) [see Fig. 4(a)]. Here we choose $\omega \ll \Lambda' \ll \Lambda_b$. This guarantees that Λ' is large enough for the trap levels to be treated as a continuum, but small enough not to probe the short-range bound-state structure. Such a choice is possible since $l_{\rm HO}$ is much greater than the microscopic lengths characterizing the intermolecular interactions. As a consequence of this choice, for the n in the truncated low-energy Hilbert space we have $W_{nb} = w_b M_n/l_{\rm HO}^{3/2}$ for some w_b. To leading order in $1/\Lambda'$ we find

$$\begin{aligned}\hat{H}_p(\Lambda') = &\sum_{n\in\mathcal{L}(\Lambda')} \epsilon_n |n\rangle \langle n| \\ &+ \sum_{b,b'} \left(\delta_{bb'}\nu_b - \sum_{n\in\mathcal{H}(\Lambda')} \frac{W_{nb}W_{nb'}}{\epsilon_n} \right) |b\rangle \langle b'| \\ &+ \sum_{b,n\in\mathcal{L}(\Lambda')} \left(\frac{w_b M_n}{l_{\rm HO}^{3/2}} |n\rangle \langle b| + \text{H.c.} \right), \end{aligned} \qquad (43)$$

where the sets $\mathcal{L}(\Lambda')$ and $\mathcal{H}(\Lambda')$ are the n with $\epsilon_n < \Lambda'$ and $\epsilon_n > \Lambda'$, respectively. In the last term W_{nb} is replaced with $w_b M_n/l_{\rm HO}^{3/2}$, which is valid because the sum is only for $\epsilon_n < \Lambda'$

and our choice of Λ' is small enough for it to be valid. The couplings are all finite.

To complete our derivation, we show that the effective Hamiltonian at scale Λ' for the physical Hamiltonian $\hat{H}_p(\Lambda')$ can be matched by $\hat{H}_{\rm eff}(\Lambda')$, the effective Hamiltonian associated with $\hat{H}_{\rm rel}$. The only apparent difference is in the middle term, the coefficient of $|b\rangle\langle b'|$. To recast the two Hamiltonians in the same form, we calculate the sum $\mathcal{S} = -\sum_{n\in\mathcal{H}(\Lambda')}(W_{nb}W_{nb'})/\epsilon_n$ appearing in Eq. (43). We split the sum into two pieces $\mathcal{S} = \mathcal{S}_1 + \mathcal{S}_2$: (i) $\mathcal{S}_1$ sums in an energy range from Λ' to $\Lambda^\star$, where $\Lambda^\star$ is chosen so that below $\Lambda^\star$ the bound-state structure is not probed and the factorization $W_{nb} = w_b M_n / l_{\rm HO}^{3/2}$ is valid, and (ii) $\mathcal{S}_2$ sums from $\Lambda^\star$ to ∞. The first sum is $\mathcal{S}_1 = -w_b w_{b'}\sqrt{\mu^3/2}(\sqrt{\Lambda^\star} - \sqrt{\Lambda'})$. The second term is finite and independent of Λ'; we denote it by $f_{b,b'}$. Thus we can write $\mathcal{S} = w_b w_{b'}\sqrt{\mu^3\Lambda'/2} + g_{b,b'}$ where $g_{b,b'}$ is finite and independent of the cutoff Λ'. With this evaluation of $\mathcal{S}$, we see that the effective Hamiltonians $\hat{H}_p(\Lambda')$ and $\hat{H}_{\rm rel}(\Lambda)$ differ only by the $g_{b,b'}$ term in the former. We can diagonalize the matrix consisting of the ν_b and $g_{b,b'}$ terms; following this basis transformation to a basis $\overline{|b\rangle}$, one obtains

$$\begin{aligned}\hat{H}_p(\Lambda') = &\sum_{n\in\mathcal{L}(\Lambda')} \epsilon_n |n\rangle\langle n| \\ &+ \sum_{b,b'}\left(-\delta_{bb'}\bar{\nu}_b - \sqrt{\frac{\mu^3\Lambda}{2}}\bar{w}_b\bar{w}_{b'}\right)\overline{|b\rangle\langle b'|} \\ &+ \sum_{b,n\in\mathcal{L}(\Lambda')}\left(\frac{\bar{w}_b M_n}{l_{\rm HO}^{3/2}}|n\rangle\langle b| + \text{H.c.}\right),\end{aligned} \tag{44}$$

where $\bar{w}_b$ and $\bar{\nu}_b$ are the couplings following the basis transformation. Note that we have chosen the factors involved in the diagonalization such that the transformed basis vectors and couplings do not depend on the cutoff. Identifying the $\overline{|b\rangle}$, $\bar{w}_b$, and $\bar{\nu}_b$ in Eq. (44) with the $|b\rangle$, w_b, and $\nu_b^\star$ in Eq. (40), we see that $\hat{H}_p(\Lambda')$ exactly coincides with $\hat{H}_{\rm rel}(\Lambda')$.

To summarize, we have shown that we are able to use an effective model that ignores the true structure of the couplings W_{nb} at high energy and assumes that the zero-range bound-state approximation is valid to determine the couplings $W_{nb} = w_b M_n / l_{\rm HO}^{3/2}$ for all n. The cost is to add diverging bound-state–bound-state couplings. Upon doing this, our Hamiltonian exactly reproduces the low-energy observables of the true physical Hamiltonian.

V. DERIVATION OF THE LATTICE MODEL

In this section we derive the multichannel Hubbard model (2) starting from a microscopic continuum description. Namely, the continuum description of our model may be written as

$$\hat{H} = \hat{H}_{\rm internal} + \hat{H}_{\rm kin} + \hat{H}_{\rm latt} + \hat{H}_{\rm couple}. \tag{45}$$

Here $\hat{H}_{\rm internal}$ is the Hamiltonian of the internal energy of the molecules and BCCs, which can be written in terms of the molecular annihilation field operators $\hat{\psi}_s(\mathbf{r})$ and the BCC annihilation field operators $\hat{\psi}_{b;\rm BCC}(\mathbf{r})$ as

$$\begin{aligned}\hat{H}_{\rm internal} = &\sum_b \int d\mathbf{r}\, E_b \hat{\psi}^\dagger_{b;\rm BCC}(\mathbf{r})\hat{\psi}_{b;\rm BCC}(\mathbf{r}) \\ &+ \sum_s \int d\mathbf{r}\, E_s \hat{\psi}^\dagger_s(\mathbf{r})\hat{\psi}_s(\mathbf{r}),\end{aligned} \tag{46}$$

where E_b is the energy of BCC state $|b\rangle$ and E_s is the energy of open-channel internal state $|s\rangle$. The next term

$$\begin{aligned}\hat{H}_{\rm kin} = &-\sum_s \int d\mathbf{r}\, \hat{\psi}^\dagger_s(\mathbf{r})\frac{1}{2m}\nabla^2\hat{\psi}_s(\mathbf{r}) \\ &-\sum_b \int d\mathbf{r}\, \hat{\psi}^\dagger_{b;\rm BCC}(\mathbf{r})\frac{1}{4m}\nabla^2\hat{\psi}_{b;\rm BCC}(\mathbf{r}),\end{aligned} \tag{47}$$

with m the molecular mass, is the kinetic energy operator. The next term is the lattice potential energy, given by

$$\begin{aligned}\hat{H}_{\rm latt} = &\sum_s \int d\mathbf{r}\, \hat{\psi}^\dagger_s(\mathbf{r})V(\mathbf{r})\hat{\psi}_s(\mathbf{r}) \\ &+ \sum_b \int d\mathbf{r}\, \hat{\psi}^\dagger_{b;\rm BCC}(\mathbf{r})2V(\mathbf{r})\hat{\psi}_{b;\rm BCC}(\mathbf{r}),\end{aligned} \tag{48}$$

with $V(\mathbf{r})$ a periodic lattice potential. For simplicity, throughout this section we assume that the lattice is "magic" in the sense that the depth is independent of the internal state of the NRMs. This is an excellent approximation for hyperfine states and can be achieved for rotational states through polarization [37] or electric field [100] control. Such magic lattices are desirable for reducing dephasing due to spatially inhomogeneous light shifts. Our model can be straightforwardly generalized to nonmagic conditions. We also take the polarizability of the BCCs equal to twice the molecular polarizability; the consequences of relaxing this condition are explored in Ref. [83]. Finally, the last term in the Hamiltonian,

$$\hat{H}_{\rm couple} = \sum_{b,s,s'}\int d\mathbf{r}[\hat{\psi}^\dagger_{b;\rm BCC}(\mathbf{r})W_{s,s',b}\hat{\psi}_s(\mathbf{r})\hat{\psi}_{s'}(\mathbf{r}) + \text{H.c.}], \tag{49}$$

is the pairing of two NRMs via a short-range coupling with matrix elements $W_{s,s',b}$ to form a BCC. Similar continuum resonance models have been used to model Feshbach resonances for ultracold atoms in optical lattices [101–107].

To derive a lattice model from the continuum description above, we expand the field operators in a complete set of localized Wannier functions; we denote the Wannier functions of the molecules by $w_{i,n,s}(\mathbf{r})$ and those of the BCCs by $\mathcal{W}_{i,n_b,b}(\mathbf{r})$, where i is the site index and n and n_b are band indices. Explicitly, these expansions read

$$\hat{\psi}_s(\mathbf{r}) = \sum_{i,n} w_{i,n,s}(\mathbf{r})\hat{a}_{i,n,s}, \tag{50}$$

$$\hat{\psi}_{b;\rm BCC}(\mathbf{r}) = \sum_{i,n_b}\mathcal{W}_{i,n_b,b}(\mathbf{r})\hat{\mathcal{A}}_{i,n_b,b}, \tag{51}$$

where $\hat{a}_{i,n,s}$ and $\hat{\mathcal{A}}_{i,n_b,b}$ are annihilation operators acting on the associated Fock spaces for molecules and BCCs, respectively.

With these definitions and under conditions analogous to those required for the validity of the Hubbard model

description for atoms, specifically that (i) tunneling can be truncated to nearest neighbors, (ii) all molecules not in short-range bound states are in the lowest band of the lattice, (iii) tunneling of the BCCs can be neglected, and (iv) pairing processes (i.e., matrix elements of $\hat{H}_{\text{couple}}$) occurring between molecules on different lattice sites can be neglected, we find the multichannel Hubbard model

$$\hat{H} = \hat{H}_{\text{on-site}} - J \sum_{\langle i,j\rangle,s} [\hat{a}^\dagger_{i,s}\hat{a}_{j,s} + \text{H.c.}], \tag{52}$$

where $\hat{a}_{i,s} \equiv \hat{a}_{i,0,s}$ and $\langle i,j\rangle$ denotes a sum over nearest-neighbor pairs i and j. Justifications for the conditions (i)–(iv) will be given shortly. In Eq. (52) the on-site Hamiltonian is

$$\hat{H}_{\text{on-site}} = \sum_{i,n,s} E_{n,s}\hat{n}_{i,n,s} + \sum_{i,n_b,b} \mathcal{E}_{n_b,b}\hat{\mathcal{N}}_{i,n_b,b} + \sum_{i,s,s',b,n,n',n_b} \left[W^{n,n',n_b}_{s,s',b}\hat{\mathcal{A}}^\dagger_{i,n_b,b}\hat{a}_{i,n,s}\hat{a}_{i,n',s'} + \text{H.c.}\right], \tag{53}$$

with molecule energies $E_{n,s} = \varepsilon_n + E_s$, ε_n the average of the band structure for band n over the first Brillouin zone, BCC energies $\mathcal{E}_{n_b,b} = E_b + \varepsilon_{n_b}$, $\hat{n}_{i,n,s} = \hat{a}^\dagger_{i,n,s}\hat{a}_{i,n,s}$, $\hat{\mathcal{N}}_{i,n_b,b} = \hat{\mathcal{A}}^\dagger_{i,n_b,b}\hat{\mathcal{A}}_{i,n_b,b}$, and we have defined the overlap integrals

$$J = -\int d\mathbf{r}\, w_{i,0,s}(\mathbf{r})\left[-\frac{1}{2m}\nabla^2 + V(\mathbf{r})\right] w_{j,0,s}(\mathbf{r}), \tag{54}$$

$$W^{n,n',n_b}_{s,s',b} = W_{s,s',b}\int d\mathbf{r}\, \mathcal{W}_{i,n_b,b}(\mathbf{r}) w_{i,n,s}(\mathbf{r}) w_{i,n',s'}(\mathbf{r}), \tag{55}$$

in which $w_{j,0,s}(\mathbf{r})$ is a nearest neighbor of $w_{i,0,s}(\mathbf{r})$.

We now turn to the justification of the conditions (i)–(iv) above. Condition (i) is standard for atomic Hubbard models and follows from the exponential decrease of tunneling amplitude with distance tunneled. Condition (ii) is reasonable for near-term experiments, in which molecules are created from ultracold atomic gases in the lowest band and transfer of population to higher bands during molecule formation can be ignored [72,108]. Also, while the complex dynamics of $\hat{H}_{\text{on-site}}$ can involve mixing between bands, such configurations only exist on the scale of a single lattice site. Condition (ii) only requires that NRMs in higher bands occur only in such short-range bound configurations and are not free to propagate through the lattice.

To illustrate the validity of (iii) and (iv), we will specialize to the case of a simple cubic lattice, for which $V(\mathbf{r}) = V\sum_{\nu=x,y,z}\sin^2(\pi\nu/a)$ with a the lattice spacing. Because of the additive separability of this lattice potential, tunneling occurs only along the principal axes. The nearest-neighbor tunneling amplitude along a principal axis, determined by a fit to numerically generated data in the range $V/E_R \geqslant 2$, is

$$\frac{J}{E_R} \approx 1.363\left(\frac{V}{E_R}\right)^{1.057}\exp(-2.117\sqrt{V/E_R}), \tag{56}$$

where $E_R = \pi^2/2ma^2$ is the recoil energy. For the BCCs, the recoil energy is half that of a molecule and the depth roughly twice, so the ratio V/E_R is four times larger than for molecules. In light of the exponential dependence of tunneling on lattice depth, this makes the tunneling of BCCs negligible compared to the tunneling of molecules. For example, the tunneling of BCCs is $\sim$1% of the molecular tunneling for a molecular lattice depth of $V \sim 8E_R$. However, we stress that although the tunneling rate of BCCs is significantly smaller than that of molecules, BCCs and molecules have the same harmonic-oscillator trapping frequency, as the increase in the lattice depth and mass cancel in $\omega = 2\sqrt{VE_R}$, within the approximation that the polarizability of BCCs is twice that of molecules.

We now turn to the matrix elements of $\hat{H}_{\text{couple}}$. These separate into a coupling constant $W_{s,s',b}/a^{3/2} \sim w_b/a^{3/2}$ with units of energy and a dimensionless geometric integral. For on-site coupling, this dimensionless integral is $I_{n_b;n,n'} = a^{3/2}\int d\mathbf{r}\, \mathcal{W}_{i,n_b,b}(\mathbf{r}) w_{i,n,s}(\mathbf{r}) w_{i,n',s'}(\mathbf{r})$. In the approximation where each site is a harmonic well, which becomes exact as $V \to \infty$, this geometric integral has the scaling $\sim l_{\text{HO}}^{-3/2} = (V/E_R)^{3/8}$; a fit to numerical data in the range $V/E_R \in [12,45]$ yields $I_{0;0,0} \sim (V/E_R)^{0.42}$, in reasonable agreement. For the off-site pairing term, the most relevant geometric integral is $\tilde{I} = a^{3/2}\int d\mathbf{r}\, \mathcal{W}_{i,0,b}(\mathbf{r}) w_{i,0,s}(\mathbf{r}) w_{i+1,0,s'}(\mathbf{r})$, in which $w_{i+1,0,s'}(\mathbf{r})$ is shifted from $w_{i,0,s}(\mathbf{r})$ by a single lattice spacing along one principal axis. We find numerically that the scaling of this integral is $\tilde{I} \sim 0.36(\frac{V}{E_R})^{0.16}\frac{J}{E_R}$ and so is much smaller than the on-site coupling. In addition to the geometric integral being small, the actual magnitude of this process is small even compared to tunneling because of the disparity in energy scales $(w_b/a^{3/2})/E_R \ll 1$. Hence, in contrast to resonance models for broad Feshbach resonances, in which off-site pairing of molecules is a key process [102,105,106], due to the narrowness of the resonances experienced by NRMs (set by the high density of BCCs at zero energy [14–16,83]), such processes are irrelevant and can be safely ignored.

We next turn to the solution of $\hat{H}_{\text{on-site}}$, which encapsulates the complex short-range physics that occurs on the length scale of a single site. For simplicity, we solve $\hat{H}_{\text{on-site}}$ in the harmonic-oscillator approximation for a single lattice site, as the separation of the center-of-mass and relative coordinates reduces the effective dimensionality of the problem. We further assume that there are never more than two molecules on a given lattice site, which occurs in many contexts, e.g., when one works close to an $n = 1$ Mott insulator (even in the adjacent strongly interacting superfluid phase), or in optical microtraps [109–111] where the number of particles can be precisely monitored. The zero-NRM and (relevant) one-NRM sectors of $\hat{H}_{\text{on-site}}$ on site i are trivially spanned by the vacuum $|0\rangle_i$ and $\hat{a}^\dagger_{i,0,s}|0\rangle_i = |s\rangle_i$, respectively. For two molecules, the Hamiltonian can be separated into center-of-mass and relative coordinates and yields $\hat{H}_{\text{c.m.}}$ and $\hat{H}_{\text{rel}}$ given in Eq. (6) and the surrounding discussion. We note that the pairing in the relative coordinate Hamiltonian depends on the internal state configuration of the open-channel NRMs indexed by s and s' and the zero of energy is taken to be $E_s + E_{s'}$. The regularization of this on-site Hamiltonian was discussed in detail in Sec. IV. Here we only need to note that the two-particle relative coordinate solutions have the general form (s-wave coupling assumed)

$$|\alpha\rangle_i = \sum_{n,s,s'} p_{\alpha;n,s,s'}|n,\ell=0\rangle|s,s'\rangle_i + \sum_b q_{\alpha;b}|b\rangle_i \tag{57}$$

and energies E_α.

With the two-body solution in hand, we can derive an effective model that is valid at low on-site density by considering only on-site configurations in which there is no molecule (vacuum state $|0\rangle_i$), a single molecule in one of the open-channel states $\hat{a}^\dagger_{i,s}|0\rangle = |s\rangle_i$, or one of the two-molecule eigenstates $|\alpha\rangle_i$ which is near resonance with two separated molecules on the scale of the coupling. We do so by noting that we can reexpress doubly occupied sites as

$$\hat{a}^\dagger_{i,s'}|s\rangle_i = P_{s,s'}\sqrt{1+\delta_{s,s'}}|s,s'\rangle_i \tag{58}$$

$$= \sum_\alpha P_{s,s'}\sqrt{1+\delta_{s,s'}}\,{}_i\langle\alpha|s,s'\rangle_i|\alpha\rangle_i, \tag{59}$$

by using the completeness of two-molecule eigenstates $|\alpha\rangle_i$.[1] Here the square-root factor, which only contributes for identical bosons, accounts for Bose stimulation, we can identify ${}_i\langle\alpha|s,s'\rangle_i \equiv p_{\alpha;0,s,s;} = \mathcal{O}^{s,s'}_\alpha$ as the opacity, and $P_{s,s'}$ accounts for on-site fermionic exchange and Pauli blocking. It is 1 for bosons and

$$P_{s,s'} = \begin{cases} 0, & s = s' \\ 1, & s > s' \\ -1, & s < s' \end{cases} \tag{60}$$

for fermions. Hence, we can concisely capture the low-filling constraint by defining modified operators as

$$\hat{c}^\dagger_{i,s} = \hat{b}^\dagger_{i,s} + \sum_\alpha\sum_{s'}\sqrt{1+\delta_{s,s'}}P_{ss'}\mathcal{O}^{s,s'}_\alpha\hat{d}^\dagger_{i,\alpha}\hat{b}_{i,s'}, \tag{61}$$

where $\hat{d}^\dagger_{i,\alpha}$ is a hard-core bosonic operator that creates an NRM pair in the eigenstate $|\alpha\rangle_i$ and $\hat{b}^\dagger_{i,s} = \hat{\mathcal{P}}^{(1)}\hat{a}^\dagger_{i,s}\hat{\mathcal{P}}^{(0)}$ with $\hat{\mathcal{P}}^{(n)}$ a projector onto the subspace with exactly n NRMs on a site. On different sites the operators $\hat{c}_{i,s}$ are defined to have the same (anti)commutation relations as the "bare" operators $\hat{a}_{i,s}$. In can be verified that this construction is the same as Eqs. (3)–(5) above. In terms of these operators, the tunneling term in Eq. (52) with the low-filling constraint becomes

$$-J\sum_{\langle i,j\rangle,s}[\hat{a}^\dagger_{i,s}\hat{a}_{j,s} + \text{H.c.}] \to -J\sum_{\langle i,j\rangle,s}[\hat{c}^\dagger_{i,s}\hat{c}_{j,s} + \text{H.c.}]. \tag{62}$$

The on-site Hamiltonian $\hat{H}_{\text{on-site}}$ can be similarly transformed to the low-filling subspace by defining number operators $\hat{n}_{i\alpha} = |\alpha\rangle_i\langle\alpha|_i$ and $\hat{n}_i = \sum_s |s\rangle_i\langle s|_i + 2\sum_\alpha |\alpha\rangle_i\langle\alpha|_i$ to write

$$\hat{H}_{\text{on-site}} \to \sum_i\left(\sum_\alpha U_\alpha\hat{n}_{i,\alpha} + \frac{3\omega}{2}\hat{n}_i\right), \tag{63}$$

where we have partitioned the energy of a two-molecule eigenstate into interaction and trap components as $E_\alpha = U_\alpha + 3\omega/2$ by defining $U_\alpha = E_\alpha - 3\omega/2$. Putting the tunneling and on-site terms together, we arrive at Eq. (2).

[1]This relation also assumes that the matrix element connecting the relevant spherical harmonic-oscillator quantum numbers and band quantum numbers (Talmi-Moshinsky coefficient) is unity. This is the case for the $|n_{\text{c.m.}} = 0\rangle$ center-of-mass state, the $|n = 0\rangle$ relative coordinate state, and the lowest band; for other motional configurations an additional overlap integral is required.

To give some physical insight into the processes occurring in this multichannel resonance model (Fig. 1), it is useful to replace the definitions of the low-filling operators into Eq. (2) to find

$$\hat{H} = \sum_i\left[\sum_\alpha U_\alpha\hat{d}^\dagger_{i\alpha}\hat{d}_{i\alpha} + \frac{3}{2}\omega\left(\sum_s\hat{b}^\dagger_{i,s}\hat{b}_{i,s} + 2\sum_\alpha\hat{d}^\dagger_{i\alpha}\hat{d}_{i\alpha}\right)\right]$$
$$- J\sum_{\langle i,j\rangle}\sum_s\left[\left(\hat{b}^\dagger_{i,s} + \sum_{\alpha,s'}\sqrt{1+\delta_{s,s'}}P_{ss'}\mathcal{O}^{s,s'}_\alpha\hat{d}^\dagger_{i\alpha}\hat{b}_{i,s'}\right)\right.$$
$$\left.\times\left(\hat{b}_{j,s} + \sum_{\alpha',s''}\sqrt{1+\delta_{s,s''}}P_{ss''}\mathcal{O}^{s,s''}_{\alpha'}\hat{d}_{j\alpha'}\hat{b}^\dagger_{j,s''}\right) + \text{H.c.}\right]. \tag{64}$$

The first line is the on-site energy, which correctly reproduces the $3\omega/2$ trap energy of each molecule and the additional U_α interaction energy when two NRMs share a lattice site. The second line consists of three different tunneling processes that can be organized according to powers of the opacities $\mathcal{O}^{s,s'}_\alpha$. The first process is tunneling of an NRM from a singly occupied site to an unoccupied site, given by the term in the second line with only $\hat{b}$ operators. This process occurs at the bare tunneling rate J. The next-order process is tunneling of a molecule from singly occupied site to another site that also contains a single molecule (and its Hermitian conjugate). This process ends with two molecules on a single site and so the resulting state is projected onto the two-molecule eigenstates $|\alpha\rangle_i$, yielding a single factor of the opacity $\mathcal{O}^{s,s'}_\alpha$. Hence, the tunneling of NRMs onto occupied sites occurs at the slower rates $\mathcal{O}^{s,s'}_\alpha J$. The final process is when a doubly occupied site and a neighboring singly occupied site exchange positions and is described by the product of the terms involving $\hat{d}$ operators in the second line. Here, operationally, the doubly occupied site is projected from the two-body eigenstates $|\alpha\rangle_i$ into open-channel states $|s,s'\rangle$, giving one factor of the opacity $\mathcal{O}^{s,s'}_\alpha$, one of the open-channel NRMs tunnels to join the neighboring site in state $|s''\rangle$, and then this two-molecule state is projected onto eigenstates $|\alpha'\rangle_i$, yielding an additional factor of the opacity $\mathcal{O}^{s,s''}_{\alpha'}$. This correlated exchange occurs at the rate $\mathcal{O}^{s,s'}_\alpha\mathcal{O}^{s,s''}_{\alpha'}J$, which is typically much slower than either of the other two tunneling processes. We note that no tunneling occurs between neighboring sites when both contain two molecules due to our low-filling constraint.

VI. CONCLUSION AND OUTLOOK

We have derived an effective multichannel Hubbard model describing ultracold nonreactive molecules in an optical lattice, starting from a fully microscopic description of two interacting NRMs in terms of their four constituent atoms. Namely, from the formal four-atom description, we derived a multichannel model for two NRMs in a harmonic trap and discussed how to properly regularize this model to remove divergences associated with zero-range closed-channel couplings. From the solutions of this two-body model, we then derived an effective many-body lattice model under the constraints of no more than two molecules per lattice site by coupling the long-wavelength physics of NRMs in the lowest band with the two-NRM on-site

description. In addition, we generalized the effective model beyond the description in Ref. [14] to include multiple internal states, such as hyperfine, rotational, or vibrational excitations, which are required to describe emerging experiments with fermionic molecules. Our work shows that the form of the multichannel Hubbard model (2) is more general than the approximations used in Ref. [14] to derive it. We also note that while the present focus has been on NRMs, we expect that a similar microscopic analysis, and hence the same effective model, holds for other systems that display a large density of resonant states at low scattering energy, such as have recently been observed [112–115] in highly magnetic atoms [116–120].

The present work clearly identifies that the form of the effective model (2) may be considered as exact, although with unknown parameters, e.g., the interaction energies U_α, and provides a formal means to determine these parameters from a fully microscopic description. However, determining the effective model parameters by this means is a daunting task and so other, approximate methods are desired. One such framework for obtaining statistical distributions for the effective model parameters based on combining random matrix theory, quantum defect theory, and transition state theory was presented in Ref. [14], building on earlier ideas from Refs. [15,16]. While this framework is expected to capture the qualitative structure of the model parameters, their quantitative values and the consequences of their breakdown are less certain. In future work, it will be interesting to study this framework critically, in order to provide a computationally tractable means for obtaining effective model parameters and setting expectations for NRM experiments. Reference [83] begins this examination. In addition, the breakdown of one or more of these approximations can provide insight into the general validity of these ubiquitous approximations in cold collisions and chemical physics.

In addition, while the present work defines the appropriate effective model, we have not investigated its many-body properties in any detail. We expect that the multichannel interaction of Eq. (2) can lead to significant qualitative differences in many-body physics compared to the ordinary single-channel Hubbard model. Future many-body calculations of the equilibrium and nonequilibrium physics of Eq. (2) in reasonable parameter regimes may lead to new many-body phenomena that are not present in systems without complex collisions.

ACKNOWLEDGMENTS

We thank Jose D'Incao, Kevin Ewart, Paul Julienne, and Brandon Ruzic for useful discussions. K.R.A.H. acknowledges the Aspen Center for Physics, which is supported by National Science Foundation Grant No. PHY-1066293, for its hospitality while part of this work was performed. This work was supported with funds from the Welch Foundation, Grant No. C-1872. M.L.W. acknowledges support from the NRC postdoctoral fellowship program.

[1] D. DeMille, Quantum Computation with Trapped Polar Molecules, Phys. Rev. Lett. **88**, 067901 (2002).
[2] G. Quéméner and P. S. Julienne, Ultracold molecules under control! Chem. Rev. **112**, 4949 (2012).
[3] P. F. Weck and N. Balakrishnan, Dynamics of chemical reactions at cold and ultracold temperatures, J. Phys. B **39**, S1215 (2006).
[4] N. Balakrishnan and A. Dalgarno, Chemistry at ultracold temperatures, Chem. Phys. Lett. **341**, 652 (2001).
[5] M. Tomza, Energetics and Control of Ultracold Isotope-Exchange Reactions between Heteronuclear Dimers in External Fields, Phys. Rev. Lett. **115**, 063201 (2015).
[6] O. Dulieu and C. Gabbanini, The formation and interactions of cold and ultracold molecules: New challenges for interdisciplinary physics, Rep. Prog. Phys. **72**, 086401 (2009).
[7] M. L. González-Martínez, O. Dulieu, P. Larrégaray, and L. Bonnet, Statistical product distributions for ultracold reactions in external fields, Phys. Rev. A **90**, 052716 (2014).
[8] R. V. Krems, Cold controlled chemistry, Phys. Chem. Chem. Phys. **10**, 4079 (2008).
[9] L. D. Carr, D. DeMille, R. V. Krems, and J. Ye, Cold and ultracold molecules: Science, technology and applications, New J. Phys. **11**, 055049 (2009).
[10] M. A. Baranov, M. Dalmonte, G. Pupillo, and P. Zoller, Condensed matter theory of dipolar quantum gases, Chem. Rev. **112**, 5012 (2012).
[11] M. L. Wall, K. R. A. Hazzard, and A. M. Rey, *From Atomic to Mesoscale: The Role of Quantum Coherence in Systems of Various Complexities* (World Scientific, Singapore, 2015), Chap. 1.
[12] A. V. Gorshkov, S. R. Manmana, G. Chen, J. Ye, E. Demler, M. D. Lukin, and A. M. Rey, Tunable Superfluidity and Quantum Magnetism with Ultracold Polar Molecules, Phys. Rev. Lett. **107**, 115301 (2011).
[13] A. V. Gorshkov, S. R. Manmana, G. Chen, E. Demler, M. D. Lukin, and A. M. Rey, Quantum magnetism with polar alkali-metal dimers, Phys. Rev. A **84**, 033619 (2011).
[14] A. Doçaj, M. L. Wall, R. Mukherjee, and K. R. A. Hazzard, Ultracold Nonreactive Molecules in an Optical Lattice: Connecting Chemistry to Many-Body Physics, Phys. Rev. Lett. **116**, 135301 (2016).
[15] M. Mayle, B. P. Ruzic, and J. L. Bohn, Statistical aspects of ultracold resonant scattering, Phys. Rev. A **85**, 062712 (2012).
[16] M. Mayle, G. Quéméner, B. P. Ruzic, and J. L. Bohn, Scattering of ultracold molecules in the highly resonant regime, Phys. Rev. A **87**, 012709 (2013).
[17] M. L. Wall and L. D. Carr, Emergent timescales in entangled quantum dynamics of ultracold molecules in optical lattices, New J. Phys. **11**, 055027 (2009).
[18] M. L. Wall and L. D. Carr, Hyperfine molecular Hubbard Hamiltonian, Phys. Rev. A **82**, 013611 (2010).
[19] T. Lahaye, C. Menotti, L. Santos, M. Lewenstein, and T. Pfau, The physics of dipolar bosonic quantum gases, Rep. Prog. Phys. **72**, 126401 (2009).
[20] B. Capogrosso-Sansone, C. Trefzger, M. Lewenstein, P. Zoller, and G. Pupillo, Quantum Phases of Cold Polar Molecules in 2D Optical Lattices, Phys. Rev. Lett. **104**, 125301 (2010).

[21] T. Sowiński, O. Dutta, P. Hauke, L. Tagliacozzo, and M. Lewenstein, Dipolar Molecules in Optical Lattices, Phys. Rev. Lett. **108**, 115301 (2012).

[22] O. Dutta, M. Gajda, P. Hauke, M. Lewenstein, D.-S. Lühmann, B. A. Malomed, T. Sowiński, and J. Zakrzewski, Non-standard Hubbard models in optical lattices: A review, Rep. Prog. Phys. **78**, 066001 (2015).

[23] J. T. Bahns, W. C. Stwalley, and P. L. Gould, Laser cooling of molecules: A sequential scheme for rotation, translation, and vibration, J. Chem. Phys. **104**, 9689 (1996).

[24] M. D. Di Rosa, Laser-cooling molecules, Eur. Phys. J. D **31**, 395 (2004).

[25] E. S. Shuman, J. F. Barry, and D. DeMille, Laser cooling of a diatomic molecule, Nature (London) **467**, 820 (2010).

[26] D. J. McCarron, E. B. Norrgard, M. H. Steinecker, and D. DeMille, Improved magneto-optical trapping of a diatomic molecule, New J. Phys. **17**, 035014 (2015).

[27] M. T. Hummon, M. Yeo, B. K. Stuhl, A. L. Collopy, Y. Xia, and J. Ye, 2D Magneto-Optical Trapping of Diatomic Molecules, Phys. Rev. Lett. **110**, 143001 (2013).

[28] A. L. Collopy, M. T. Hummon, M. Yeo, B. Yan, and J. Ye, Prospects for a narrow line MOT in YO, New J. Phys. **17**, 055008 (2015).

[29] M. Yeo, M. T. Hummon, A. L. Collopy, B. Yan, B. Hemmerling, E. Chae, J. M. Doyle, and J. Ye, Rotational State Microwave Mixing for Laser Cooling of Complex Diatomic molecules, Phys. Rev. Lett. **114**, 223003 (2015).

[30] E. B. Norrgard, D. J. McCarron, M. H. Steinecker, M. R. Tarbutt, and D. DeMille, Submillikelvin Dipolar Molecules in a Radio-Frequency Magneto-Optical Trap, Phys. Rev. Lett. **116**, 063004 (2016).

[31] E. A. Shapiro, A. Pe'er, J. Ye, and M. Shapiro, Piecewise Adiabatic Population Transfer in a Molecule Via a Wave Packet, Phys. Rev. Lett. **101**, 023601 (2008).

[32] K.-K. Ni, S. Ospelkaus, M. H. G. de Miranda, A. Peér, B. Neyenhuis, J. J. Zirbel, S. Kotochigova, P. S. Julienne, D. S. Jin, and J. Ye, A high phase-space-density gas of polar molecules, Science **322**, 231 (2008).

[33] P. S. Żuchowski and J. M. Hutson, Reactions of ultracold alkali-metal dimers, Phys. Rev. A **81**, 060703 (2010).

[34] S. Ospelkaus, K.-K. Ni, D. Wang, M. H. G. de Miranda, B. Neyenhuis, G. Quéméner, P. S. Julienne, J. L. Bohn, D. S. Jin, and J. Ye, Quantum-state controlled chemical reactions of ultracold potassium-rubidium molecules, Science **327**, 853 (2010).

[35] S. Ospelkaus, A. Pe'er, K. K. Ni, J. J. Zirbel, B. Neyenhuis, S. Kotochigova, P. S. Julienne, J. Ye, and D. S. Jin, Ultracold dense gas of deeply bound heteronuclear molecules, Nat. Phys. **4**, 622 (2008).

[36] S. Ospelkaus, K. K. Ni, M. H. G. de Miranda, A. Pe'er, B. Nyenhuis, D. Wang, S. Kotochigova, P. S. Julienne, D. S. Jin, and J. Ye, Ultracold polar molecules near quantum degeneracy, Faraday Discuss. **142**, 351 (2009).

[37] B. Neyenhuis, B. Yan, S. A. Moses, J. P. Covey, A. Chotia, A. Petrov, S. Kotochigova, J. Ye, and D. S. Jin, Anisotropic Polarizability of Ultracold Polar ^{40}K^{87}Rb Molecules, Phys. Rev. Lett. **109**, 230403 (2012).

[38] M. H. G. de Miranda, A. Chotia, B. Neyenhuis, D. Wang, G. Quemener, S. Ospelkaus, J. L. Bohn, J. Ye, and D. S. Jin, Controlling the quantum stereodynamics of ultracold bimolecular reactions, Nat. Phys. **7**, 502 (2011).

[39] A. Chotia, B. Neyenhuis, S. A. Moses, B. Yan, J. P. Covey, M. Foss-Feig, A. M. Rey, D. S. Jin, and J. Ye, Long-Lived Dipolar Molecules and Feshbach Molecules in a 3D Optical Lattice, Phys. Rev. Lett. **108**, 080405 (2012).

[40] B. Zhu, B. Gadway, M. Foss-Feig, J. Schachenmayer, M. L. Wall, K. R. A. Hazzard, B. Yan, S. A. Moses, J. P. Covey, D. S. Jin, J. Ye, M. Holland, and A. M. Rey, Suppressing the Loss of Ultracold Molecules Via the Continuous Quantum Zeno Effect, Phys. Rev. Lett. **112**, 070404 (2014).

[41] B. Yan, S. A. Moses, B. Gadway, J. P. Covey, K. R. A. Hazzard, A. M. Rey, D. S. Jin, and J. Ye, Observation of dipolar spin-exchange interactions with lattice-confined polar molecules, Nature (London) **501**, 521 (2013).

[42] K. R. A. Hazzard, B. Gadway, M. Foss-Feig, B. Yan, S. A. Moses, J. P. Covey, N. Y. Yao, M. D. Lukin, J. Ye, D. S. Jin, and A. M. Rey, Many-Body Dynamics of Dipolar Molecules in an Optical Lattice, Phys. Rev. Lett. **113**, 195302 (2014).

[43] T. Takekoshi, M. Debatin, R. Rameshan, F. Ferlaino, R. Grimm, H.-C. Nägerl, C. R. Le Sueur, J. M. Hutson, P. S. Julienne, S. Kotochigova, and E. Tiemann, Towards the production of ultracold ground-state RbCs molecules: Feshbach resonances, weakly bound states, and the coupled-channel model, Phys. Rev. A **85**, 032506 (2012).

[44] M. P. Köppinger, D. J. McCarron, D. L. Jenkin, P. K. Molony, H.-W. Cho, S. L. Cornish, C. R. Le Sueur, C. L. Blackley, and J. M. Hutson, Production of optically trapped ^{87}RbCs Feshbach molecules, Phys. Rev. A **89**, 033604 (2014).

[45] P. K. Molony, P. D. Gregory, Z. Ji, B. Lu, M. P. Köppinger, C. R. Le Sueur, C. L. Blackley, J. M. Hutson, and S. L. Cornish, Creation of Ultracold ^{87}Rb ^{133}Cs Molecules in the Rovibrational Ground State, Phys. Rev. Lett. **113**, 255301 (2014).

[46] T. Takekoshi, L. Reichsöllner, A. Schindewolf, J. M. Hutson, C. R. Le Sueur, O. Dulieu, F. Ferlaino, R. Grimm, and H.-C. Nägerl, Ultracold Dense Samples of Dipolar RbCs Molecules in the Rovibrational and Hyperfine Ground State, Phys. Rev. Lett. **113**, 205301 (2014).

[47] P. K. Molony, P. D. Gregory, A. Kumar, C. R. Le Sueur, J. M. Hutson, and S. L. Cornish, Production of ultracold ^{87}Rb ^{133}Cs in the absolute ground state: Complete characterisation of the stimulated Raman adiabatic passage transfer, Chem. Phys. Chem. **17**, 3811 (2016).

[48] P. D. Gregory, J. Aldegunde, J. M. Hutson, and S. L. Cornish, Controlling the rotational and hyperfine state of ultracold ^{87}Rb ^{133}Cs molecules, Phys. Rev. A **94**, 041403 (2016).

[49] C.-H. Wu, J. W. Park, P. Ahmadi, S. Will, and M. W. Zwierlein, Ultracold Fermionic Feshbach Molecules of ^{23}Na ^{40}K, Phys. Rev. Lett. **109**, 085301 (2012).

[50] J. W. Park, S. A. Will, and M. W. Zwierlein, Two-photon pathway to ultracold ground state molecules of ^{23}Na ^{40}K, New J. Phys. **17**, 075016 (2015).

[51] J. W. Park, S. A. Will, and M. W. Zwierlein, Ultracold Dipolar Gas of Fermionic ^{23}Na ^{40}K Molecules in their Absolute Ground State, Phys. Rev. Lett. **114**, 205302 (2015).

[52] J. W. Park, Z. Z. Yan, H. Loh, S. A. Will, and M. W. Zwierlein, Second-scale nuclear spin coherence time of trapped ultracold ^{23}Na ^{40}K molecules, arXiv:1606.04184.

[53] F. Wang, X. He, X. Li, B. Zhu, J. Chen, and D. Wang, Formation of ultracold NaRb Feshbach molecules, New J. Phys. **17**, 035003 (2015).

[54] M. Guo, B. Zhu, B. Lu, X. Ye, F. Wang, R. Vexiau, N. Bouloufa-Maafa, G. Quéméner, O. Dulieu, and D. Wang, Creation of an Ultracold Gas of Ground-State Dipolar ^{23}Na ^{87}Rb Molecules, Phys. Rev. Lett. **116**, 205303 (2016).

[55] M.-S. Heo, T. T. Wang, C. A. Christensen, T. M. Rvachov, D. A. Cotta, J.-H. Choi, Y.-R. Lee, and W. Ketterle, Formation of ultracold fermionic NaLi Feshbach molecules, Phys. Rev. A **86**, 021602 (2012).

[56] S. Dutta, J. Lorenz, A. Altaf, D. S. Elliott, and Y. P. Chen, Photoassociation of ultracold LiRb* molecules: Observation of high efficiency and unitarity-limited rate saturation, Phys. Rev. A **89**, 020702 (2014).

[57] J. Deiglmayr, A. Grochola, M. Repp, K. Mörtlbauer, C. Glück, J. Lange, O. Dulieu, R. Wester, and M. Weidemüller, Formation of Ultracold Polar Molecules in the Rovibrational Ground State, Phys. Rev. Lett. **101**, 133004 (2008).

[58] J. Deiglmayr, A. Grochola, M. Repp, O. Dulieu, R. Wester, and M. Weidemüller, Permanent dipole moment of LiCs in the ground state, Phys. Rev. A **82**, 032503 (2010).

[59] B. K. Stuhl, M. T. Hummon, M. Yeo, G. Quéméner, J. L. Bohn, and J. Ye, Evaporative cooling of the dipolar hydroxyl radical, Nature (London) **492**, 396 (2012).

[60] M. Zeppenfeld, B. G. U. Englert, R. Glöckner, A. Prehn, M. Mielenz, C. Sommer, L. D. van Buuren, M. Motsch, and G. Rempe, Sisyphus cooling of electrically trapped polyatomic molecules, Nature (London) **491**, 570 (2012).

[61] S. Chervenkov, X. Wu, J. Bayerl, A. Rohlfes, T. Gantner, M. Zeppenfeld, and G. Rempe, Continuous Centrifuge Decelerator for Polar Molecules, Phys. Rev. Lett. **112**, 013001 (2014).

[62] C. Meng, A. P. P. van der Poel, C. Cheng, and H. L. Bethlem, Femtosecond laser detection of Stark-decelerated and trapped methylfluoride molecules, Phys. Rev. A **92**, 023404 (2015).

[63] M. Lemeshko, R. V. Krems, J. M. Doyle, and S. Kais, Manipulation of molecules with electromagnetic fields, Mol. Phys. **111**, 1648 (2013).

[64] M. Gröbner, P. Weinmann, F. Meinert, K. Lauber, E. Kirilov, and H.-C. Nägerl, A new quantum gas apparatus for ultracold mixtures of K and Cs and KCs ground-state molecules, J. Mod. Opt. **63**, 1829 (2016).

[65] S. Y. T. van de Meerakker, H. L. Bethlem, N. Vanhaecke, and G. Meijer, Manipulation and control of molecular beams, Chem. Rev. **112**, 4828 (2012).

[66] N. R. Hutzler, H.-I. Lu, and J. M. Doyle, The buffer gas beam: An intense, cold, and slow source for atoms and molecules, Chem. Rev. **112**, 4803 (2012).

[67] C. P. Koch and M. Shapiro, Coherent control of ultracold photoassociation, Chem. Rev. **112**, 4928 (2012).

[68] T. Köhler, K. Góral, and P. S. Julienne, Production of cold molecules via magnetically tunable Feshbach resonances, Rev. Mod. Phys. **78**, 1311 (2006).

[69] B. Gadway and B. Yan, Strongly interacting ultracold polar molecules, J. Phys. B **49**, 152002 (2016).

[70] B. Damski, L. Santos, E. Tiemann, M. Lewenstein, S. Kotochigova, P. Julienne, and P. Zoller, Creation of a Dipolar Superfluid in Optical Lattices, Phys. Rev. Lett. **90**, 110401 (2003).

[71] J. K. Freericks, M. M. Maśka, A. Hu, T. M. Hanna, C. J. Williams, P. S. Julienne, and R. Lemański, Improving the efficiency of ultracold dipolar molecule formation by first loading onto an optical lattice, Phys. Rev. A **81**, 011605 (2010).

[72] A. Safavi-Naini, M. L. Wall, and A. M. Rey, Role of interspecies interactions in the preparation of a low-entropy gas of polar molecules in a lattice, Phys. Rev. A **92**, 063416 (2015).

[73] S. A. Moses, J. P. Covey, M. T. Miecnikowski, B. Yan, B. Gadway, J. Ye, and D. S. Jin, Creation of a low-entropy quantum gas of polar molecules in an optical lattice, Science **350**, 659 (2015).

[74] S. Ospelkaus, K.-K. Ni, G. Quéméner, B. Neyenhuis, D. Wang, M. H. G. de Miranda, J. L. Bohn, J. Ye, and D. S. Jin, Controlling the Hyperfine State of Rovibronic Ground-State Polar Molecules, Phys. Rev. Lett. **104**, 030402 (2010).

[75] S. A. Will, J. W. Park, Z. Z. Yan, H. Loh, and M. W. Zwierlein, Coherent Microwave Control of Ultracold ^{23}Na ^{40}K Molecules, Phys. Rev. Lett. **116**, 225306 (2016).

[76] A. Micheli, Z. Idziaszek, G. Pupillo, M. A. Baranov, P. Zoller, and P. S. Julienne, Universal Rates for Reactive Ultracold Polar Molecules in Reduced Dimensions, Phys. Rev. Lett. **105**, 073202 (2010).

[77] Z. Idziaszek, K. Jachymski, and P. S. Julienne, Reactive collisions in confined geometries, New J. Phys. **17**, 035007 (2015).

[78] A. Simoni, S. Srinivasan, J.-M. Launay, K. Jachymski, Z. Idziaszek, and P. S. Julienne, Polar molecule reactive collisions in quasi-1D systems, New J. Phys. **17**, 013020 (2015).

[79] B. Zhu, G. Quéméner, A. M. Rey, and M. J. Holland, Evaporative cooling of reactive polar molecules confined in a two-dimensional geometry, Phys. Rev. A **88**, 063405 (2013).

[80] J. F. E. Croft and J. L. Bohn, Long-lived complexes and chaos in ultracold molecular collisions, Phys. Rev. A **89**, 012714 (2014).

[81] D. Jaksch, C. Bruder, J. I. Cirac, C. W. Gardiner, and P. Zoller, Cold Bosonic Atoms in Optical Lattices, Phys. Rev. Lett. **81**, 3108 (1998).

[82] A. Sanpera, M. Lewenstein, V. Ahufinger, B. Damski, A. Sen De, and U. Sen, Ultracold atomic gases in optical lattices: Mimicking condensed matter physics and beyond, Adv. Phys. **56**, 243 (2007).

[83] M. L. Wall, R. Mukherjee, S. S. Alam, N. P. Mehta, and K. R. A. Hazzard, Lattice model parameters for ultracold nonreactive molecules: Chaotic scattering and its limitations, following paper, Phys. Rev. A **95**, 043636 (2017).

[84] J. H. Macek, Properties of autoionizing states of He, J. Phys. B **1**, 831 (1968).

[85] C. D. Lin, Hyperspherical coordinate approach to atomic and other Coulombic three-body systems, Phys. Rep. **257**, 1 (1995).

[86] S. T. Rittenhouse, J. von Stecher, J. P. D'Incao, N. P. Mehta, and C. H. Greene, The hyperspherical four-fermion problem, J. Phys. B **44**, 172001 (2011).

[87] L. Delves, Tertiary and general-order collisions (II), Nucl. Phys. **20**, 275 (1960).

[88] Yu. F. Smirnov and K. V. Shitikova, The method of K harmonics and the shell model, Sov. J. Part. Nucl. **8**, 344 (1977).
[89] R. T. Pack and G. A. Parker, Quantum reactive scattering in three dimensions using hyperspherical (APH) coordinates. Theory, J. Chem. Phys. **87**, 3888 (1987).
[90] V. Aquilanti and S. Cavalli, The quantum-mechanical Hamiltonian for tetraatomic systems in symmetric hyperspherical coordinates, J. Chem. Soc. Faraday Trans. **93**, 801 (1997).
[91] A. Kuppermann, Reactive scattering with row-orthonormal hyperspherical coordinates. 2. Transformation properties and Hamiltonian for tetraatomic systems, J. Phys. Chem. A **101**, 6368 (1997).
[92] J. S. Avery, *Hyperspherical Harmonics: Applications in Quantum Theory* (Springer Science + Business Media, New York, 2012), Vol. 5.
[93] M. Abramowitz and I. A. Stegun, *Handbook of Mathematical Functions: With Formulas, Graphs, and Mathematical Tables* (Courier, Mineola, 1964), Vol. 55.
[94] T. Busch, B. G. Englert, K. Rzazewski, and M. Wilkens, Two cold atoms in a harmonic trap, Found. Phys. **28**, 549 (1998).
[95] O. I. Tolstikhin, S. Watanabe, and M. Matsuzawa, 'Slow' variable discretization: A novel approach for Hamiltonians allowing adiabatic separation of variables, J. Phys. B **29**, L389 (1996).
[96] J. Wang, J. P. D'Incao, and C. H. Greene, Numerical study of three-body recombination for systems with many bound states, Phys. Rev. A **84**, 052721 (2011).
[97] V. Kokoouline and F. Masnou-Seeuws, Calculation of loosely bound levels for three-body quantum systems using hyperspherical coordinates with a mapping procedure, Phys. Rev. A **73**, 012702 (2006).
[98] H. Suno, Hyperspherical slow variable discretization method for weakly bound triatomic molecules, J. Chem. Phys. **134**, 064318 (2011).
[99] C. J. Pethick and H. Smith, *Bose-Einstein Condensation in Dilute Gases* (Cambridge University Press, Cambridge, 2002).
[100] S. Kotochigova and D. DeMille, Electric-field-dependent dynamic polarizability and state-insensitive conditions for optical trapping of diatomic polar molecules, Phys. Rev. A **82**, 063421 (2010).
[101] E. Timmermans, P. Tommasini, M. Hussein, and A. Kerman, Feshbach resonances in atomic Bose-Einstein condensates, Phys. Rep. **315**, 199 (1999).
[102] L.-M. Duan, Effective Hamiltonian for Fermions in an Optical Lattice Across a Feshbach Resonance, Phys. Rev. Lett. **95**, 243202 (2005).
[103] V. Gurarie and L. Radzihovsky, Resonantly paired fermionic superfluids, Ann. Phys. (NY) **322**, 2 (2007).
[104] H. P. Büchler, Microscopic Derivation of Hubbard Parameters for Cold Atomic Gases, Phys. Rev. Lett. **104**, 090402 (2010).
[105] J. von Stecher, V. Gurarie, L. Radzihovsky, and A. M. Rey, Lattice-Induced Resonances in One-Dimensional Bosonic Systems, Phys. Rev. Lett. **106**, 235301 (2011).
[106] M. L. Wall and L. D. Carr, Microscopic Model for Feshbach Interacting Fermions in an Optical Lattice with Arbitrary Scattering Length and Resonance Width, Phys. Rev. Lett. **109**, 055302 (2012).
[107] M. L. Wall and L. D. Carr, Strongly interacting fermions in an optical lattice, Phys. Rev. A **87**, 033601 (2013).
[108] J. P. Covey, S. A. Moses, M. Gärttner, A. Safavi-Naini, M. T. Miecnikowski, Z. Fu, J. Schachenmayer, P. S. Julienne, A. M. Rey, D. S. Jin, and J. Ye, Doublon dynamics and polar molecule production in an optical lattice, Nat. Commun. **7**, 11279 (2016).
[109] A. M. Kaufman, B. J. Lester, and C. A. Regal, Cooling a Single Atom in an Optical Tweezer to its Quantum Ground State, Phys. Rev. X **2**, 041014 (2012).
[110] J. D. Thompson, T. G. Tiecke, A. S. Zibrov, V. Vuletić, and M. D. Lukin, Coherence and Raman Sideband Cooling of a Single Atom in an Optical Tweezer, Phys. Rev. Lett. **110**, 133001 (2013).
[111] N. R. Hutzler, L. R. Liu, Y. Yu, and K.-K. Ni, Eliminating light shifts in single-atom optical traps, New J. Phys. **19**, 023007 (2017).
[112] K. Baumann, N. Q. Burdick, M. Lu, and B. L. Lev, Observation of low-field Fano-Feshbach resonances in ultracold gases of dysprosium, Phys. Rev. A **89**, 020701 (2014).
[113] A. Frisch, M. Mark, K. Aikawa, F. Ferlaino, J. L. Bohn, C. Makrides, A. Petrov, and S. Kotochigova, Quantum chaos in ultracold collisions of gas-phase erbium atoms, Nature (London) **507**, 475 (2014).
[114] T. Maier, I. Ferrier-Barbut, H. Kadau, M. Schmitt, M. Wenzel, C. Wink, T. Pfau, K. Jachymski, and P. S. Julienne, Broad universal Feshbach resonances in the chaotic spectrum of dysprosium atoms, Phys. Rev. A **92**, 060702 (2015).
[115] T. Maier, H. Kadau, M. Schmitt, M. Wenzel, I. Ferrier-Barbut, T. Pfau, A. Frisch, S. Baier, K. Aikawa, L. Chomaz, M. J. Mark, F. Ferlaino, C. Makrides, E. Tiesinga, A. Petrov, and S. Kotochigova, Emergence of Chaotic Scattering in Ultracold Er and Dy, Phys. Rev. X **5**, 041029 (2015).
[116] M. Lu, S. H. Youn, and B. L. Lev, Trapping Ultracold Dysprosium: A Highly Magnetic Gas for Dipolar Physics, Phys. Rev. Lett. **104**, 063001 (2010).
[117] M. Lu, N. Q. Burdick, S. H. Youn, and B. L. Lev, Strongly Dipolar Bose-Einstein Condensate of Dysprosium, Phys. Rev. Lett. **107**, 190401 (2011).
[118] Y. Tang, N. Q. Burdick, K. Baumann, and B. L. Lev, Bose-Einstein condensation of 162 Dy and 160 Dy, New J. Phys. **17**, 045006 (2015).
[119] A. Frisch, K. Aikawa, M. Mark, A. Rietzler, J. Schindler, E. Zupanic, R. Grimm, and F. Ferlaino, Narrow-line magneto-optical trap for erbium, Phys. Rev. A **85**, 051401 (2012).
[120] K. Aikawa, A. Frisch, M. Mark, S. Baier, A. Rietzler, R. Grimm, and F. Ferlaino, Bose-Einstein Condensation of Erbium, Phys. Rev. Lett. **108**, 210401 (2012).